ELECTRICAL AND DIELECTRIC BEHAVIOUR OF ANODIC ALUMINIUM OXIDE THIN FILMS

A Thesis submitted

in Partial Fulfilment of the requirments

for the Degree of

MASTER OF TECHNOLOGY

by

SANJEEV KUMAR SINHA

to the

MATERIALS SCIENCE PROGRAMME

INDIAN INSTITUTE OF TECHNOLOGY KANPUR

November, 1994

MSP-1994-M-SIN-ELE

TO MY

PARENTS

28 11.94

CERTIFICATE

This is to certify that the research work contained in the M.Tech thesis entitled "ELECTRICAL AND DIELECTRIC BEHAVIOUR OF ANODIC ALUMINIUM OXIDE THIN FILMS" by Mr.Sanjeev Kumar Sinha has been carried out under my supervision and that has not been submitted elsewhere for a degree.

Jitendra Kumar

27th November, 1994.

(Jitendra Kumar)
Professor
Material Science Programme
Indian Institute of Technology
Kanpur

ACKNOWLEDGEMENTS

I derive esteemed pleasure in expressing my sincere gratitude to Dr.Jitendra Kumar for his invaluable guidance and cooperation during the course of this investigation.

I would like to thank Mr.Subhas Chand, Mr.Swaminathan, Mr.Atanu Saha and Mr.Santanu Bhattacharya for their valuable contribution towards the completion of my thesis.

Thanks are due to my freinds Sandeep Kumar, Gautam Kumar Roy, Atul Kumar, Binod Kumar Singh, Tripta thakur, Ivan Saha, Deb. Bannerjee and others for giving a finishing touch to my thesis and for their constant encouragement throughout the duration of my stay in the campus.

I am also grateful to my family for their constant support and for the love and affection bestowed upon me.

SANJEEV KUMAR SINHA

CONTENTS

		Page
	List of figures	vi
	List of tables	ix
	Abstract	x
CHAPTER 1	Introduction	1
	1.1 DIELECTRIC PROPERTIES	2
	1.1.1 Trilayer Structures As Capacitor	2
	1.1.2 Thin Film Capacitors	6
	1.1.3 Dissipation Factor	9
	1.2 CONDUCTION MECHANISMS	9
	1.2.1 Tunneling	10
	1.2.2 Schottky Emission	15
	1.2.3 Poole-Frenkel Effect	19
	1.2.4 High Field Emission Current	21
	1.3 OBJECTIVE OF PRESENT WORK	22
CHAPTER 2	EXPERIMENTAL DETAILS AND PROCEDURES	23
	2.1 PREPARATION OF SAMPLES	23
	2.1.1 Substrate Cleaning	23
	2.1.2 Bottom Electrode Deposition	24
	2.1.3 Anodization	24
	2.1.4 Top Layer Electrode	25
	2.1.5 Device Area Measurement	25
	2.2 CAPACITANCE MEASUREMENTS	26
	2.3 CURRENT-VOLTAGE (I-V) MEASUREMENTS	28

CHAPTER 3 RESULTS AND DISCUSSION 30

3.1 THE NATURE OF OXIDE 30

3.1.1 Oxide Formation 32

3.2 DIELECTRIC PROPERTIES 33

3.2.1 Thickness Dependence 35

3.2.2 Area Effect 44

3.2.3 Effect Of Aging 48

3.3 CURRENT-VOLTAGE CHARACTERISTICS 51

3.3.1 Conduction Process(es) 51

3.3.2 Effect Of Polarity Change 68

3.3.3 Hysteresis Effect 70

CHAPTER 4 CONCLUSIONS 72

REFERENCES 74

LIST OF FIGURES

		Page
Fig.1.1	A parallel plate capacitor with air as the dielectric.	4
Fig.1.2	A parallel plate capacitor with an oxide as the dielectric.	5
Fig.1.3	Schematic representation of the band structure of a metal-insulator-metal structure with a voltage V applied to it.	11
Fig.1.4	Energy diagram of a general barrier of metal-insulator-metal sandwich structures.	13
Fig.1.5	Rectangular potential barrier for a M-I-M structure (a) V = Ø (b) V ≤ ϕ_o/e (c) V > ϕ_o/e.	14
Fig.1.6	Energy diagram of a rectangular barrier with the image potential super imposed.	16
Fig.1.7	Energy diagram of schottky effect at a neutral contact under applied electric field.	17
Fig.1.8	Energy diagram showing the Poole-Frenkel effect at a trap centre.	20
Fig.2.1	Different stages of preparation of Al-Al_2O_3-Al trilayer structures.	26
Fig.2-2	Schematic representation of anodization set up.	27
Fig.2-3	Schematic diagram of the experimental setup for current-voltage (I-V) measurements.	29
Fig.3-1	Variation of A/C_b with thickness of a bulk capacitor with alumina as dielectric; A and C_b being its cross-sectinal area and the bulk capacitance respectively.	34

Fig.3.2 Measured capacitance (C_m) of the Al-Al_2O_3-Al structure as a function of insulator (Al_2O_3) thickness. 36

Fig.3.3 Variation of surface area / volume with thickness of the insulator. 37

Fig.3.4 Variation of area/capacitance with thickness of Al-Al_2O_3-Al structure; A being cross-sectional surface area. C_i represents the interfacial capacitance = 1.22$\mu F/cm^2$. 38

Fig.3.5 Variation of bulk capacitance (C_b) with oxide thickness in Al-Al_2O_3-Al structure. The cross-sectional area being 1.74 mm^2. 41

Fig.3.6 Variation of area/capacitance (A/C_b) with oxide thickness in Al-Al_2O_3-Al structure ; A being cross-sectional surface area and C_b the bulk capacitance. 42

Fig.3.7 Variation of area/capacitance with thickness of Al-Al_2O_3-Al structure (which is formed after heating the anodized film at 160°C for 4 hrs in air); A being the cross-sectional surface area. C_i is the interfacial capacitance. 43

Fig.3.8 Variation of area/capacitance with thickness of two Al-Al_2O_3-Al structures; one anodized and made at room temperature and other formed after heating the anodized film at 160°C for 4 hrs in air. 45

Fig.3.9 Measured capacitance (C_m)of Al-Al_2O_3-Al structure as a function of oxide thickness for two cross-sectional areas. 46

Fig.3.10 Interfacial capacitance (C_i) of Al-Al_2O_3-Al structures (formed after heating the anodized film at 200°C for 4 hrs in air) as a function of time for cross-sectional areas 0.83mm^2 and 1.74mm^2. 49

Fig.3.11 Measured capacitance (C_m) of Al-Al_2O_3-Al structures (formed after heating the anodized film at 200°C for 4 hrs in air) as a function of time for three different thicknesses. 50

Fig.3.12 Increased thickness of Al_2O_3 after ten days of aging. 52

Fig.3.13 Current density (J) versus voltage (V) characteristics of Al-Al_2O_3-Al structures for various oxide thicknesses. 53

Fig.3.14 Variation of resistance (Ω-cm^2) with thickness of Al-Al_2O_3-Al structures for various oxide thicknesses. 57

Fig.3.15 The ln J versus $V^{1/2}$ characteristics of Al-Al_2O_3-Al structures for various oxide thicknesses. 59

Fig.3.16 The ln J/V versus $V^{1/2}$ characteristics of Al-Al_2O_3-Al structures for various oxide thicknesses. 60

Fig.3.17 Variation of $\beta_{pf}/d^{-1/2}$ with $d^{-1/2}$; β_{pf} is the field lowering coefficient and d is the oxide thickness. 64

Fig.3.18 The ln J/V^2 versus 1/V characteristics of Al-Al_2O_3-Al structures for various oxide thicknesses. 66

Fig.3.19 Various current processes found in Al-Al_2O_3-Al structures with their range of operation. 67

Fig.3.20 Effect of polarity change on J-V characteristics of Al-Al_2O_3-Al structures. 69

Fig.3.21 Effect of hysteresis on J-V characteristics of Al-Al_2O_3-Al structures. 71

LIST OF TABLES

Table Page

3.1 Measured capacitance C_m as a function of oxide thickness . 47

3.2 Characteristics of various conduction modes for thin insulating films . 55

3.3 Threshold voltages of Al-Al_2O_3-Al structure . 56

3.4 Voltage ranges of different conduction mechanisms . 61

3.5 Different parameters obtained for Schottky emission . 63

ABSTRACT

The studies relating to the electrical characteristics of Metal-Insulator-Metal structures have received considerable attention in recent past from both fundamental and application viewpoints. This has happened primarily because M-I-M structures show useful electrical and dielectric properties and have found application as charge storage capacitors, switching devices, cold cathode emitters, etc. The properties of the intermediate insulating film layer, interfacial effects and nature of the electrodes largely determine the overall behaviour of such structures. Due to the large number of the variables present, the exact nature of the physical processes involved are still not well understood. Of particular interest is the Al-Al_2O_3-Al system. An attempt has been made in the present study to investigate its electrical and dielectric properties by varying the thickness of the intermediate oxide layer. For precise control of thickness, vacuum evaporated aluminium films have been anodized (upto a certain depth only) in 3 wt% tartaric acid solution of pH5.5. The top electrode, also of aluminium, was made by thermal deposition in vacuum ~ 10^{-6} torr using suitable masks to obtain junctions of nearly 1mm X 1mm and 1.4mm X 1.4mm areas. The capacitance and the current density-voltage (J-V) characteristics have been measured and analysed.

The inverse areal capacitance of Al-Al_2O_3-Al trilayer structures is shown to vary linearly with oxide thickness (d)

giving a non zero intercept at d = Ø. This amounts to a significant interfacial capacitance ~ 1.22 μF /cm^2 which is in series with the bulk capacitance of Al_2O_3. Moreover, it is shown that annealing of the oxide layer at 16Ø°C and 2ØØ°C improves the dielectric characteristics considerably, as the capacitance gets stabilized and dielectric constant corresponds to 9.Ø and 1Ø.9, respectively. However, the interfacial capacitance increases and takes a value of 1.36 $\mu F/cm^2$ after annealing at 16Ø°C for four hours in air.

The capacitance of Al-Al_2O_3-Al structure varies directly with the cross-sectional area like that of the bulk capacitor. Current-voltage (J-V) , ln J vs $V^{1/2}$ ln (J/V) vs $V^{1/2}$ and ln (J/V^2) vs 1/V plots have revealed the possible current conduction mechanisms as ohmic, Schottky, Poole-Frenkel and field assisted tunneling in different voltage regimes, range of which depend on the oxide thickness and shift towards higher voltages. The barrier height(ϕ_o) is shown to increase with thickness and takes a value of Ø.69 eV for 26ØA thick Al_2O_3. Also, the field lowering coefficient for the Poole-Frenkel effect is found to be 2.1Ø X $1Ø^{-5}$ $V^{1/2}m^{-1/2}$. Finally, evidence has been given to suggest that the nature of the barrier/interfaces are different and hysteresis occurs in the current density versus voltage curve beyond a threshold value.

1. INTRODUCTION

Metal-insulator-metal structures (M-I-M) have been studied extensively and have made rapid progress during the past three decades, mainly, due to the ever increasing development of thin film devices. These M-I-M structures utilise the thin film technology and have the advantage of space, weight, power saving along with reliability and rugged construction. Also, they have vast applications as switching devices, charge storage capacitors, cold cathode emitters, etc. Most of the devices work on the passage of current through thin layers of materials [1-3]. Although numerous studies have been undertaken in this area, yet, the effect of aging on capacitance is still not well understood. Moreover, electrical conduction in thin insulating films continues to be the area of investigation with regard to the exact nature of the processes involved .

Of particular interest are the M-I-M structures with oxide insulators such as Al_2O_3, Ta_2O_5, and SiO_2 because of their unique properties. It is believed that the electrical properties of such structures depend mainly on the nature of the intermediate insulating layer and the associated interfacial effects. The electrical conduction through M-I-M structures have been largely investigated in two ways. In the first, metal-oxide-metal strucures have been examined with oxide layer (thickness < 100A) grown by thermal oxidation of the base electrode. Very high electric field across them causes drifting of ions, electrons, etc. through thin insulating films (e.g., Al_2O_3 in $Al-Al_2O_3-Al$) and

gives rise to measurable currents. Their I-V characteristics are used to determine the actual conduction process(es). The parameters that influence the behaviour are the oxide thickness, interface barrier height, temperature and the nature of contacts (with the impurities distribution, if any) of the insulator with the metal electrodes. In the second, the anomalous behaviour involving permanent increase in the electrical conductivity, caused by the application of the critical potential across the M-I-M structures, has been studied. Such a phenomenon is termed as `forming process' [4-6], and is distinguished by a pronounced voltage controlled negative resistance. In addition, studies concerning the capacitance of such sandwiched structures have been undertaken.

The observed characteristics of the M-I-M structures have indeed been utilised to develop switching elements, memory devices, cold cathode emitters, etc. [1]. Although, various theories have been proposed to explain the processes involved, but, none of these is found adequate to account for all the observed characteristics [6-9].

1.1 DIELECTRIC PROPERTIES

1.1.1 *Trilayer structures as capacitor*

A capacitor consists of two conductors (usually metal plates) physically separated from each other by vacuum, air or some

insulating material. The two conductors usually are the same and so provide a symmetrical structure with so called identical interfaces. Such an arrangement leads to I-V characteristics which are independent of the direction of applied field (i.e.,same with forward and reverse bias). When a potential (V) is applied across the structure, an electric field E is developed between the two plates (Fig 1.1), such that

$$E = V/d \ , \quad V = E.d$$

and the capacitance` C´ is given by

$$C = Q/V = Q/E.d \qquad , \qquad ....(1.1)$$

where `Q´ is the charge on each conductor, and `d´ is the separation between the plates. From Gauss´s law , the electric field E is given by

$$E = Q/(\varepsilon_o A) \qquad , \qquad ....(1.2)$$

where ε_o is the permittivity of free space. Thus,

$$C = \varepsilon_o A/d \qquad ....(1.3)$$

When a dielectric is present between the two conductors, application of voltage causes polarization which, in turn, develops a small electric field opposite to that of the applied field (Fig 1.2). Thus the voltage gets reduced to V/K, if `K´ is

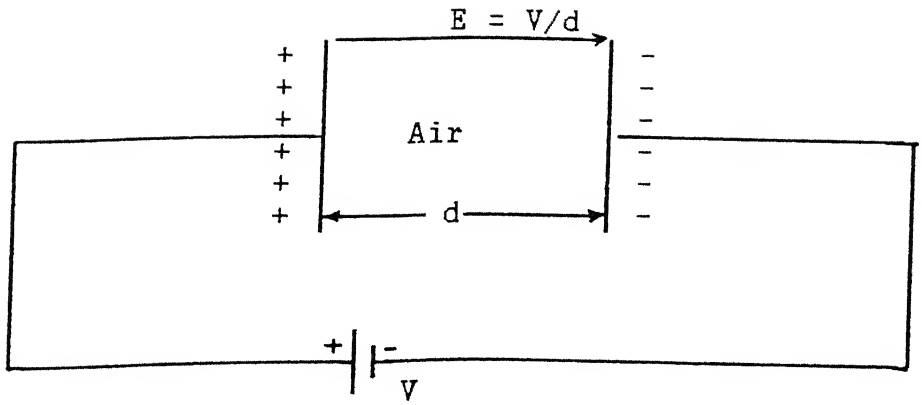

Fig 1.1 A parallel plate capacitor with air as the dielectric.

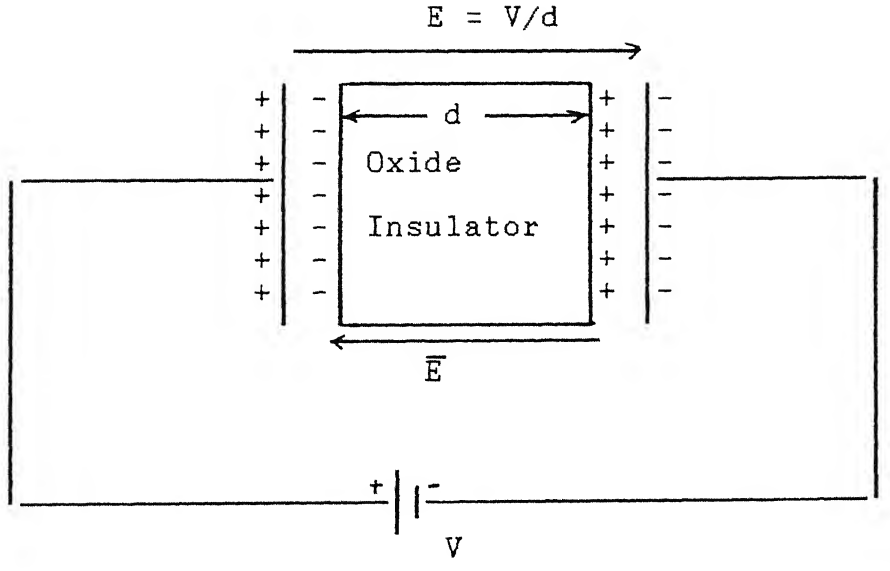

Fig 1.2 A parallel plate capacitor with an oxide as a dielectric.

the dielectric constant of the material. In other words, the charges appearing on the dielectric surfaces due to polarization attract further charges from the battery. Thus, the total charge accumulated on the conductor plates becomes larger for the same voltage, resulting in a higher value of capacitance (eq. 1.1). The bulk capacitance (C_b) of the dielectric is therefore given by

$$C_b = \epsilon_o K A / d \qquad \ldots.(1.4)$$

1.1.2 *Thin film capacitors*

It consists of a very thin film (thickness ~ 100A) of some dielectric material (say, alumina) sandwiched between two metal film electrodes of thickness ~ 2500A. Such a metal-insulator-metal (M-I-M) structure acts as a capacitor alright, but, exhibits certain peculiar properties as well, e.g., interfacial capacitance, asymmetry in I-V characteristics with polarity reversal, etc. For an ideal behaviour, the nature of top and bottom interfaces should be the same both in physical and chemical terms. However, the technique usually adopted for making thin film capacitors leads to non ideal characteristics. As, for example, alumina formed by oxidation/anodization of the bottom aluminium electrode upto a certain depth (~ few tens of A) results in an intimate (or continuous) contact at the metal-oxide interface. On the other hand, the top contact becomes abrupt as the evaporation of aluminium is made afterwards over alumina surface.

Recently Hebard, Ajuria and Eick [10] have found that the reciprocal areal capacitance (A/C_m) of a Al-Al_2O_3-Al thin film trilayer structure varies linearly with the dielectric thickness (d) following the equation

$$A/C_m = A/C_i + d/(\varepsilon_o K) \qquad \ldots.(1.5)$$

where C_m is the measured capacitance, C_i is the interfacial capacitance, A is the junction area and the last term stands for A/C_b(Eq.1.4). This description is different from the case of a general parallel plate capacitor in the sense that a constant interfacial term is added to the bulk capacitance. That means A/C_m versus 'd' plot no longer passes through origin, but, makes an intercept with the ordinate. It is believed that the electrical charges or the potential drops near the interfaces are responsible for the emergence of this extra term. The situation is equivalent to having two capacitors with interfacial and bulk capacitance values in series. Obviously, use of eq.(1.4) to estimate the insulator thickness from the measured capacitance, is not at all justified, as it leads to higher value than the actual. Therefore, studies relating to variation of capacitance with insulator thickness got initiated in the past. This became further necessary after discrepency was observed between the thickness of the insulating films (d) determined by capacitance measurements and the thickness values (d_t) actually required for explaining the I-V characteristics. Therefore, arbitrary relations have been used for determining d_t e.g., $d = 3d_t$ [3] and $d = (1.5 \text{ to } 2.0)d_t$ [11]. Later investigations have attributed the effect to the electrical

field penetration into the region of the metal electrodes [12,13,14]. There are, however, serious objections to this interpretation [15] due to unknown electric field boundary conditions at the metal-dielectric interface. Chow [16] used the existence of non-uniform thickness of insulating film to explain the tunnel characteristics of the M-I-M structure. Hurych [17] has shown that 1/C exhibits a non-linear behaviour for $d_u < 5q$, where d_u is some critical thickness and q is a positive constant of the order of angstrom unit. Also, 1/C has a positive non-zero intercept at $d_u = \emptyset$.

Recently, Krupski [18] employed a specular reflection model and took into account the quantum effects to find the screened electrostatic potential in a M-I-M structure. The resulting interfacial capacitance was found to be in semi-quantitative agreement with the experimental value of Hebard et.al. [1Ø] for $Al-Al_2O_3-Al$ capacitor. Also, X-Ray photoelectron spectroscopic observations have provided evidence for the presence of an electrical double layer at the interfaces. This, not only, changes the work function of the metal and the barrier shape at the interface, but also, influences the polarisation of the molecules and hence the dielectric properties of the insulator significantly [18].

1.1.3 *Dissipation Factor*

The dissipation factor `D´ can be written as

$$D = \{K''(w)/K'(w)\} + d/\{w\,K'(w)\,\varepsilon_o A\,R_o\} \qquad .....(1.6)$$

where $K(w) = K'(w) + K''(w)$, ε_o is permittivity, w is 2π times the frequency, and R_o the d.c resistance of the M-I-M structure. In eq.(1.6), the first term accounts for the dielectric loss (tan δ) and second accounts for the conduction processes, such as tunneling and thermally activated hopping, which become important as $d \to 0$ [10,23]. The value of the dissipation factor thus gives a direct idea about the loss of the insulator. Accordingly, if the dissipation factor is small the dielectric is considered to be good as it amounts to low loss and high resistance R_o.

1.2 CONDUCTION MECHANISMS

Electric current in M-I-M structures may result by the movement of ions and/or electrons. Ionic conduction occurs due to the presence of defects and their drift under the influence of the applied field. But, as the ionic mobilities are very low, the contribution of ions to the total current is negligible [24]. Application of a small potential across the M-I-M structure amounts to high electric field in the dielectric region due to its thickness being very small(a few tens of A). The electronic conduction is, therefore, associated with high electric fields and

can be divided into two classes [24,27] :

(i) *Barrier limited processes* - tunneling, Schottky emission, thermionic field emission, and
(ii) *Bulk limited processes* - space-charge limited currents, Poole Frenkel effect, internal field ionisation, impurity conduction.
All these current processes are presented schematically in Fig 1.3. A brief account of them now follows :

1.2.1 *Tunneling* :

If energy of an electron is less than the interfacial potential barrier and the potential barrier is very thin (~ 50 A), the quantum mechanical wave function has a non-zero value in a region beyond the barrier. This means that the electron has a finite probability of penetrating the barrier. This phenomenon is known as tunneling.

Simmons [28 , 29] evaluated the transmission coefficients for a general barrier of height (ϕ) and width (s) using the WKB approximation. The relationship between the tunnel current density and applied voltage at absolute zero is written as

$$J = J_o \{\phi \exp(-A\phi^{1/2}) - (\phi + eV) \exp[-A(\phi + eV)^{1/2}]\} , \quad \ldots.(1.7)$$

where $J_o = e/2\pi h\, s^2$ and $A = (4\pi s/h)(2m)^{1/2}$, s is the width of the barrier at Fermi level, h is the Plancks constant, e the charge

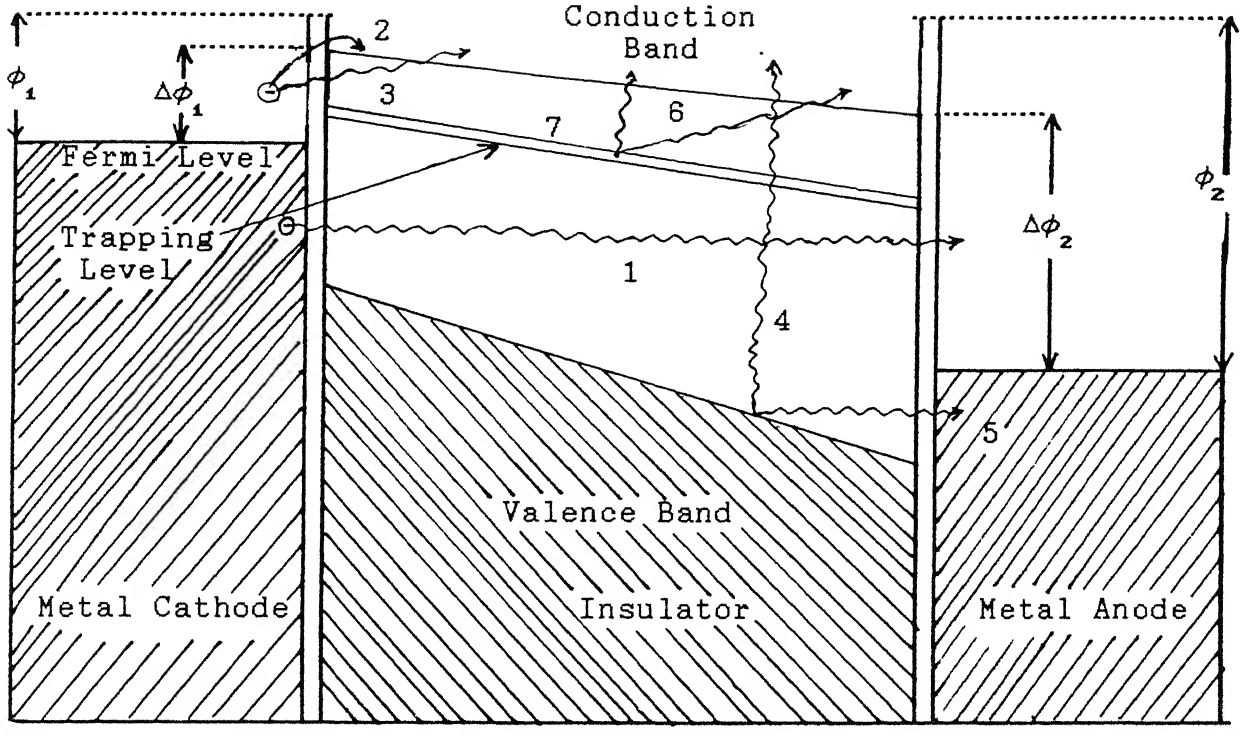

Fig 1.3 Schematic representation of the band structure of a metal-insulator-metal structure with a voltage V. ϕ_1 & ϕ_2 are the two metal work functions ; $\Delta\phi_1$ & $\Delta\phi_2$ are the potential steps from metal to insulator conduction bands.

(1) Direct tunneling of electrons from one metal to the other.

(2) Thrmionic (Schottky) emission over a contact barrier.

(3) Tunneling through the barrier.

(4) At high temperature and small forbidden gap electrones rise directly from valence band to conduction band.

(5) Tunneling from valence band into metal directly.

(6) Thermal excitation from trap levels into the conduction band of ions.

(7) Tunneling from trap levels in the insulator into metal

and V is the applied voltage. Since the current density changes marginally with temperature, the above expression can also be used at higher temperatures. Moreover, this can be applied to any shape of the potential barrier provided the mean barrier height(ϕ) is known. For a rectangular barrier shown in Fig (1.4), expression (1.7) leads to the following results :

(i) at low-voltage (V ~ Ø),

$$J = J_o A \phi_o^{1/2}(eV) \exp(-A \phi_o^{1/2}) \quad \ldots.(1.8)$$

Here ϕ_o = work function of the metal. Thus eq.(1.8) expresses J as a linear function of V; that is, the junction is ohmic for very low voltages.

(ii) at intermediate voltages, $V \leq \phi_o/e$, so

$$J = J_o \{ (\phi_o - (eV/2)) \exp[-A(\phi_o - (eV/2))^{1/2}] - (\phi_o + (eV/2))\exp[-A(\phi_o + (eV/2))^{1/2}] \quad \ldots.(1.9)$$

(iii) at high voltages, $V \geq \phi_o/e$,

$$J = J_o (2.2 (eV)^2 / 4 \phi_o) \{ \exp[-2 A \phi_o^{3/2}/(2.96 eV)] - (1 +(2 eV /\phi_o)) \exp[(-2A \phi_o^{3/2}/(2.96 eV)) (1 +(2 eV /\phi_o)^{1/2}]\} \quad \ldots.(1.10)$$

Fig 1.5(a-c) illustrates the energy diagram for the three situation given above.

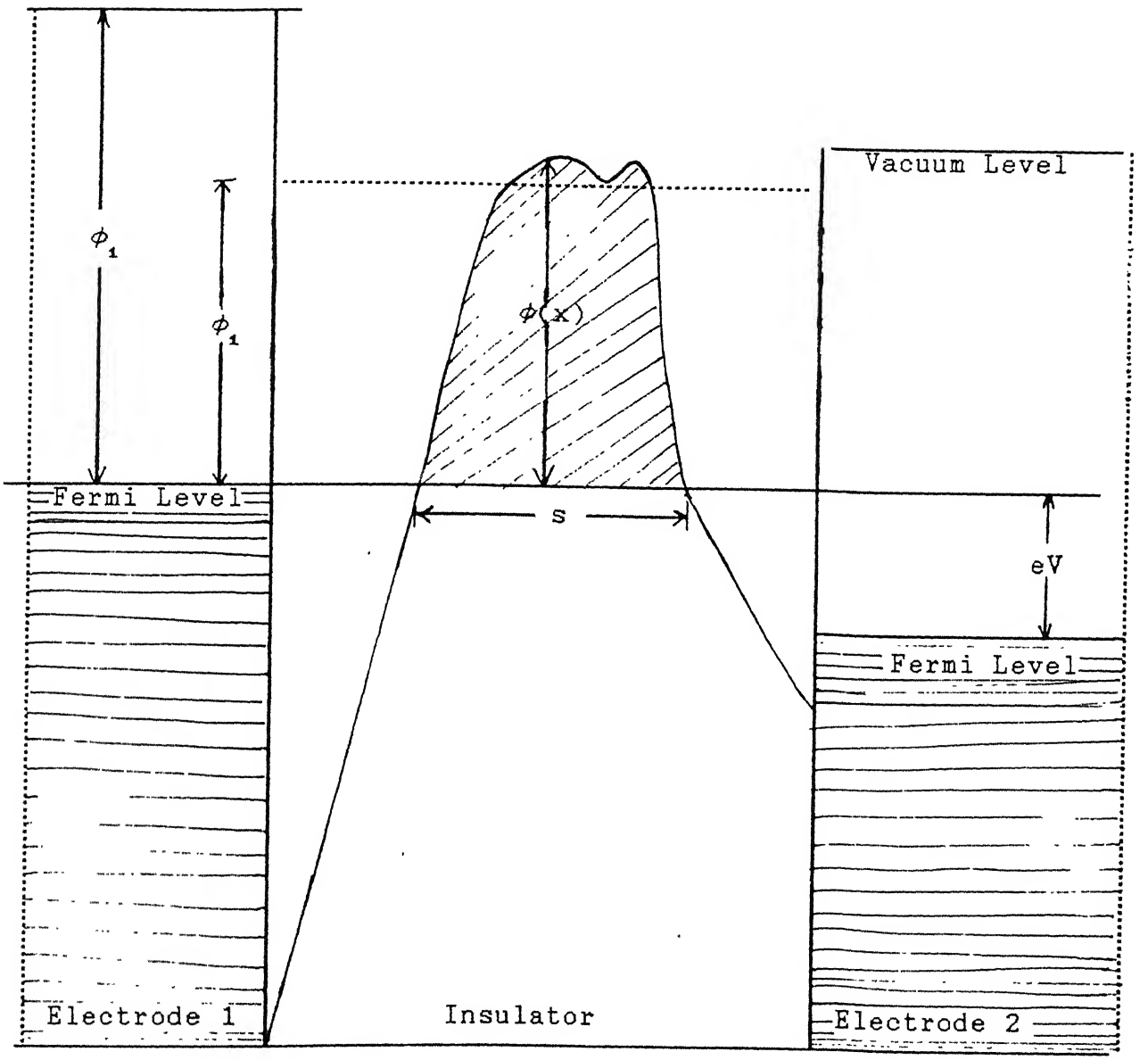

Fig 1.4 Energy diagram of a general barrier of M-I-M (metal-insulator-metal) sandwich structure

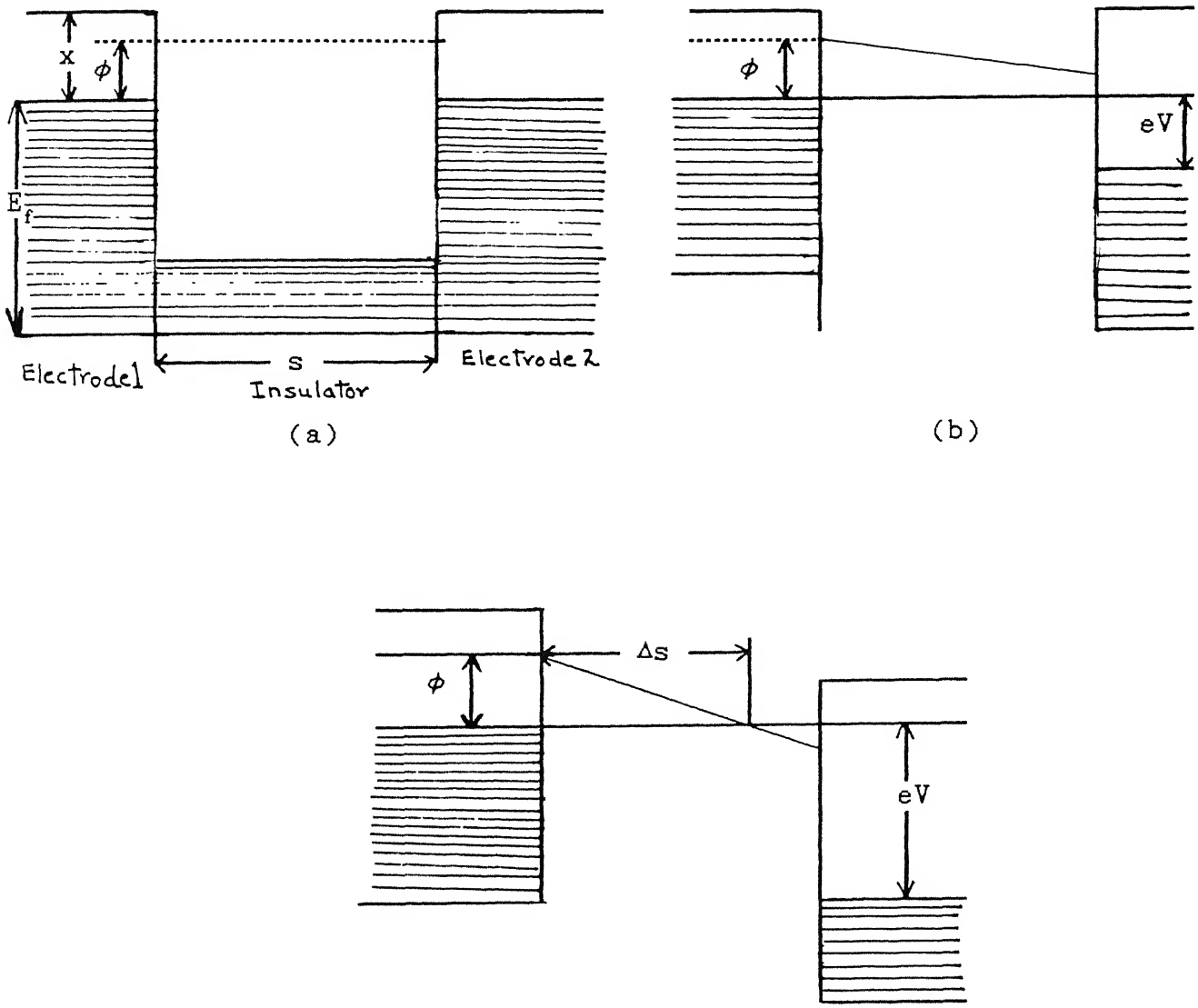

Fig 1.5 Rectangular potential barrier for a M-I-M structure

(a) V = Ø

(b) $V \leq \phi_o/e$

(c) $V \geq \phi_o/e$

(iv) at very high voltages i.e. $V >> \phi_o/e$,

$$J = J_o \{2.2\ (eV)^2 /(4\phi_o)\} \exp [\ (-2A\ \phi_o^{3/2}\ )/(2.96\ eV)\ ] \quad ....(1.11)$$

This is a Fowler-Nordheim equation. Fig 1.6 shows the energy band diagram of a rectangular symmetrical barrier [30]. It may be pointed out that the effect of the image force is to round off the barrier corners and reduce its height and the width [31].

1.2.2 *Schottky emission*

Due to the presence of high fields across the insulating films the potential barrier is effectively reduced with the result that the electrons possessing energy greater than the reduced barrier may escape into the conduction band of the insulator. This is called the Schottky emission [Fig 1.7]. Consider an electron at a distance x from the surface of an uncharged metal. The only force on the electron is the classical image force which is attractive in nature. Thus, the potential energy(ϕ_{im}) of the electron due to image force is given by

$$\phi_{im} = -e^2/(16\pi\ \varepsilon_o K^*\ x\ )$$

Here K^* is high frequency dielectric constant. For a rectangular barrier of height ϕ_o, the potential step at a distance x' from interface becomes

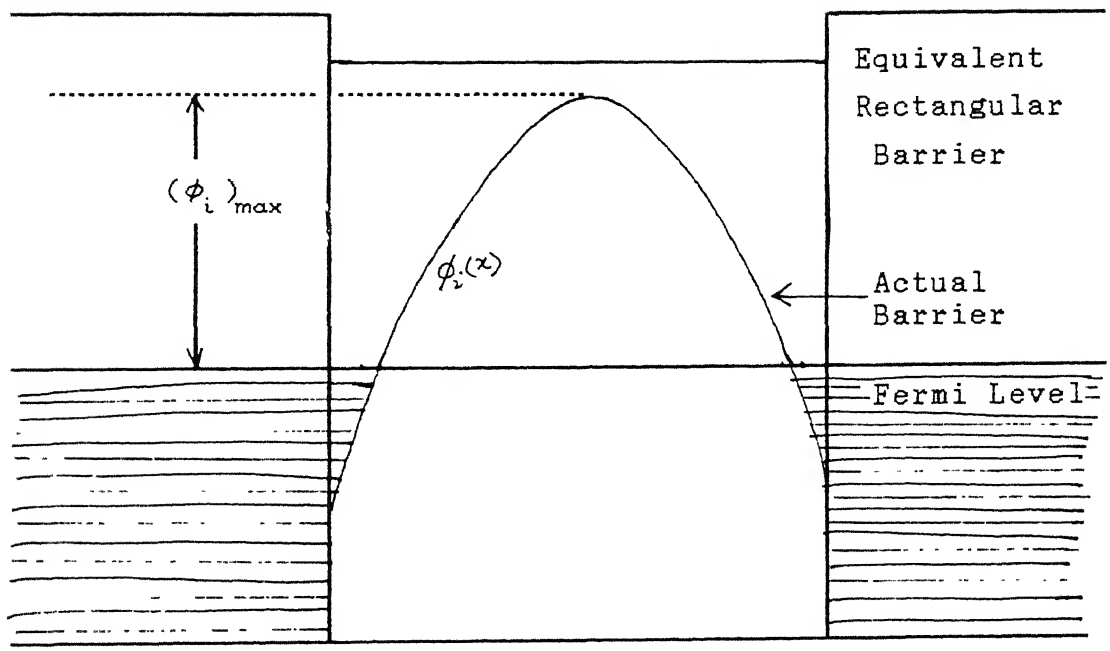

Fig 1.6 Energy diagram of a rectangular barrier with image potential superimposed.

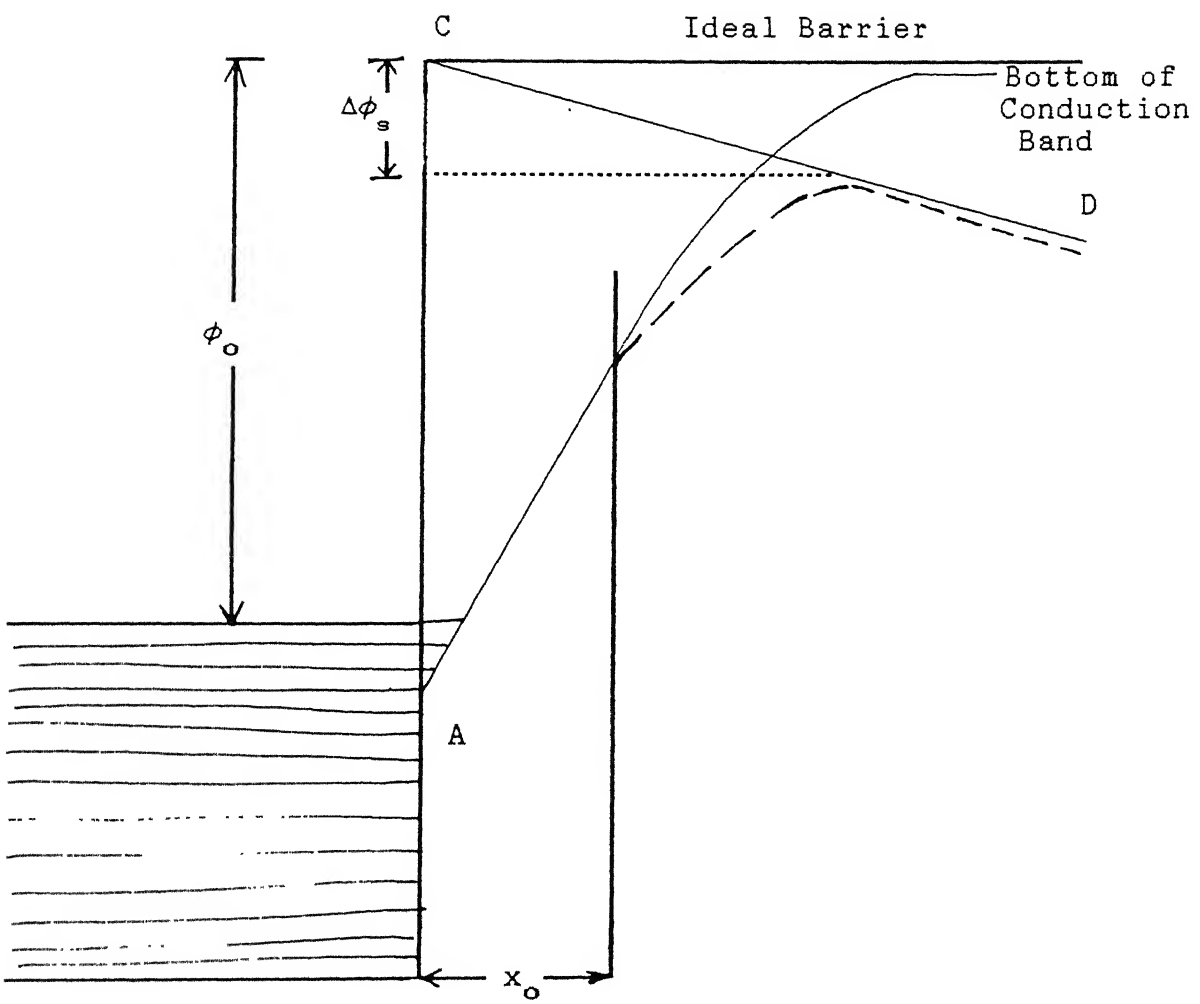

Fig 1.7 Energy diagram of Schottky effect at a neutral contact under applied electric field.

$$\phi(x) = \phi_o + \phi_{im} = \phi_o - [e^2/(16\pi\ \varepsilon_o\ K^*\ x)]$$

$\phi(x)$ is shown by curve AB in Fig 1.7. The image force is effective only beyond a distance having some critical value x_o.

The electric field resulting due to applied voltage (V) across the metal-insulator junctions further lowers the potential barrier. The total change ($\Delta\phi_s$) in the barrier height (ϕ) is given by

$$\Delta\phi_s = [e^3/(4\pi\ K^*\ \varepsilon_o)]^{1/2}\ (V/d)^{1/2} = \beta_s(V/d)^{1/2} \quad ....(1.12)$$

Now the total current across the M-I-M structure is given by Richardson-Schottky expression [32,14]

$$J = A_s T^2\ \exp -[(\phi_o - \Delta\phi_s)/(kT)]$$

Substituting the value of $\Delta\phi_s$ from equation (1.12), we get

$$J = A_s T^2 \exp\ [-\phi_o/(kT)]\ \exp\ [\beta_s(V/d)^{1/2}/(kT)] \quad ....(1.13)$$

where $A_s = 4\pi$ me $(k)^2/(h^3)$ is the Richardson - Dushman constant, $\beta_s = e^3/(4\pi\ K^*\ \varepsilon_o)^{1/2}$ is the Schottky conduction coefficient, and 'd' stands for the thickness of the insulator. Thus, the Schottky current, unlike the tunneling current, is temperature dependent. So, when log J is plotted against $V^{1/2}$, the linear portion (if any) may correspond to Schottky emission. This effect was first observed in Al-Al_2O_3-Al structure by Emptage and Tantraporn [33].

Pollack [34] analysed the temperature and voltage dependence of current and found the results in agreement with the expression(1.13).

1.2.3 *Poole-Frenkel effect*

This process is the bulk analogue of the Schottky effect and involves lowering of the trap barrier in the bulk of an insulator. The schematic diagram of the Poole-Frenkel effect is given in Fig (1.8). The extent of the trap barrier lowering is given by

$$\Delta\phi_{pf} = [e^3/(\pi\ \varepsilon_0\ K^*)]^{1/2}(V/d)^{1/2} = \beta_{pf}(V/d)^{1/2} \quad ....(1.14)$$

Comparison of expressions (1.12) and (1.14) clearly shows that the barrier lowering in Poole-Frenkel effect is twice to what is found in the case of Schottky emission.

The field assisted thermal emission-limited current due to the Poole-Frenkel effect is given by

$$J = A_{pf}(V/d)\ \exp\ [-\phi_0/(kT)]\ \exp\ [\beta_{pf}(V/d)^{1/2}/(kT)] \quad ....(1.15)$$

where A_{pf} is a constant. This type of conduction was observed by Vermilyae [35]. Simmons [36] assumed that both traps and donors are present in the insulator and modified Poole-Frenkel contribution to the current to

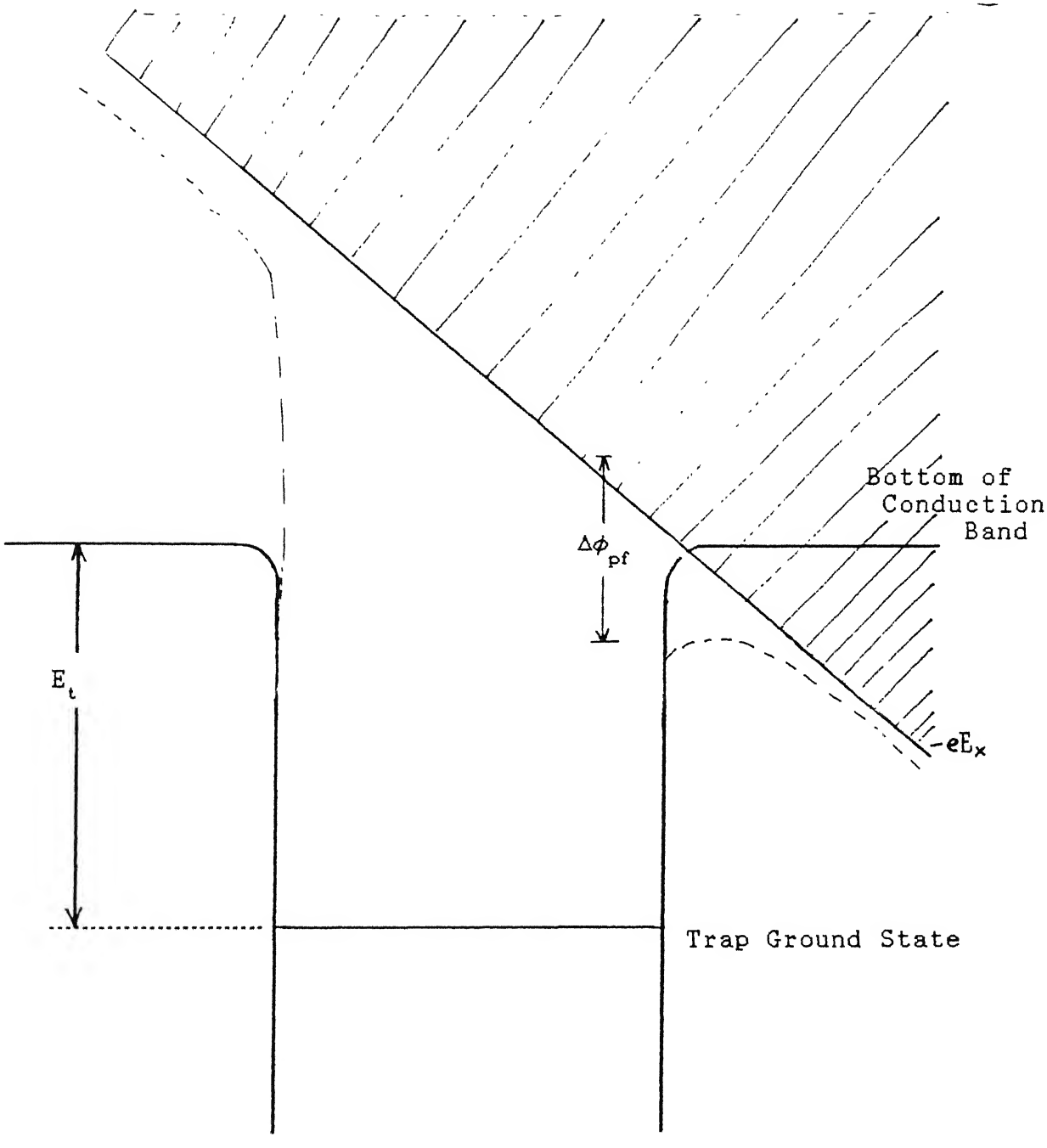

Fig 1.8 Energy diagram showing the Poole-Frenkel effect at a trap centre.

$$J = A_{pf}(V/d) \exp [-\phi_o/(kT)] \exp [\beta_{pf}(V/d)^{1/2}/(2kT)] \quad ....(1.16)$$

It is interesting to note that although $\Delta\phi_{pf} = 2\Delta\phi_s$, the coefficient of $(V/d)^{1/2}$ in the exponential is the same for both the Richardson-Schottky (eq.1.13) and Poole-Frenkel J-V characteristics, since $\beta_{pf}/2 = \beta_s$. The equation essentially gives the same dependence of current density on voltage as seen in the Schottky effect. Yet, the difference is that while the Schottky emission is electrode limited, the current contribution due to Poole-Frenkel effect is bulk limited. Moreover, the electrode limited process cannot continue indefinitely because the bulk resistance decreases more slowly with increase in voltages than does the electrode contact resistance. Hence, at voltages beyond a transition value V_t (at which contact resistance falls to bulk value), the current is essentially controlled by the bulk [26,36,37].

1.2.4 *High field emission current*

An insulator which contains no donors and is sufficiently thick to inhibit tunneling does not normally conduct. However, if an ohmic contact is made to the insulator, electrons from the electrode can be injected into the conduction band of the insulator. This gives rise to space charge, which in turn, controls the electron injection thereafter. The net current that flows through the insulator is termed as space-charge limited

(SCL) current. But, as the applied voltage reaches a critical value, the ohmic contact no longer exists at the metal-insulator interface. Further increase in voltage gives rise to an emission limited current rather than space charge limited current [30]. The current beyond the critical voltage is given by Mott and Gurney law [38],

$$J \propto V^2 / d^3$$

where d is the thickness of the oxide layer. If the insulator contains traps, a large fraction of the injected space charge will condense therein to cause a decrease in the free-carrier density [39] and hence the current as well.

1.3 OBJECTIVE OF THE PRESENT WORK

Although a lot of experimental studies have been undertaken on the Al-Al_2O_3-Al structures, yet, the understanding of their capacitance and current-voltage (I-V) characteristics is far from complete. This makes the Al-Al_2O_3-Al system still relevant and curious for further investigation. Attempt has, therefore, been made here to study Al-Al_2O_3-Al structures with regard to capacitance, current voltage characteristics and dielectric stability as a function of oxide thickness (range being 26A-260A). The basic aim has been to separate out the interfacial capacitance, find out the associated changes on annealing and determine the conduction mechanisms.

2. EXPERIMENTAL DETAILS AND PROCEDURES

This chapter deals with the procedures followed for the preparation of the Al-Al_2O_3-Al trilayer structures, measurements of their capacitance and recording of their current voltage (I-V) characteristics.

2.1 PREPARATION OF SAMPLES

2.1.1 *Substrate cleaning*

The first step in thin film device fabrication technology is the preparation of smooth, clean and undamaged substrate surfaces. The substrates used here were the microscopic slides and great care was taken in cleaning them. The task was to remove the commonly encountered contaminations such as oil, fingerprints, airborne articulate matter, residues from manufacturing and packaging, etc [26]. For this the glass slides of size 75 mm X 25 mm X 1 mm were first cleaned with a soap detergent and then dipped in chromic acid for some time. After rinsing in distilled water, they were cleaned in solutions of trichloro ethylene, acetone, methanol and distilled water in succession using an ultrasonic cleaner. Subsequently, they were dried by an electric air blower. Finally, the slides were wiped with lint free tissue paper and transferred to a vacuum chamber for storage.

2.1.2 *Bottom electrode deposition*

Aluminium of 99.999% purity was deposited onto the glass substrate by thermal evaporation technique under vacuum using a mask strip of size 75 mm X 1 mm (Fig 2.1 a). The thickness of aluminium layer deposited was ~ 25ØØA. For evaporation a precleaned tungsten boat was used. After loading the aluminium charge in the basket inside the work chamber the evaporation was carried out at a pressure of about 5 X $1Ø^{-6}$ torr by passing a low voltage high current through the filament for about 8-1Ø seconds. The glass slides were thereafter removed and electrical connection made on one end of the aluminium strip using conducting silver paste as shown in fig 2.1(b).

2.1.3 *Anodization*

This technique was used to form the oxide layer over the aluminium strips deposited on the glass slides. For this, a solution of 3 wt % tartaric acid in deionised water having pH 5.5 (adjusted with NH_4OH solution) was used as the electrolyte [4Ø-42]. The aluminium strip was made the anode while a stainless steel plate of size 1ØØ mm X 4Ø mm X 1 mm served as cathode. The electrodes were connected to a constant voltage constant current power supply (Aplab CVCC, Ø-3ØV, Ø-1A). The anodization was carried out for two minutes at a particular voltage. The current that flows causes the dissociation of tartaric acid and the resulting oxygen ions get attracted towards the anode. The

combination of aluminium and oxygen ion takes place at the anode and a continuous oxide film of uniform thickness develops upto a certain depth of the aluminium strip (Fig 2.2). The samples were then cleaned with distilled water and dried with an air blower. The thickness of the oxide was controlled and varied by selecting the voltage for anodization (Fig 2.1c). In order to ensure stability of the oxide layer, the samples after anodization were kept in an oven at 160°C or 200°C for 4 hours.

2.1.4. *Top layer electrode*

After annealing the glass slides were again returned to the evaporator. The top aluminium electrode of about 2500A thickness was then deposited through a mask attached to the slide. The electrical contacts from this elctrode were made as before using the conducting silver paste. The contacts were allowed to dry by leaving the samples in air for about 3-4 hours. The samples were then ready for measurements (Fig 2.1d).

2.1.5. *Device area measurement*

To find out the true area of the sandwiched trilayer structure an image analyser [Leitz ASM 68K with VARIOSCAN V16 camera] was used. The area of the sample was measured after due magnification to third place of decimal and recorded. Each area was measured thrice and then the precise value was recorded.

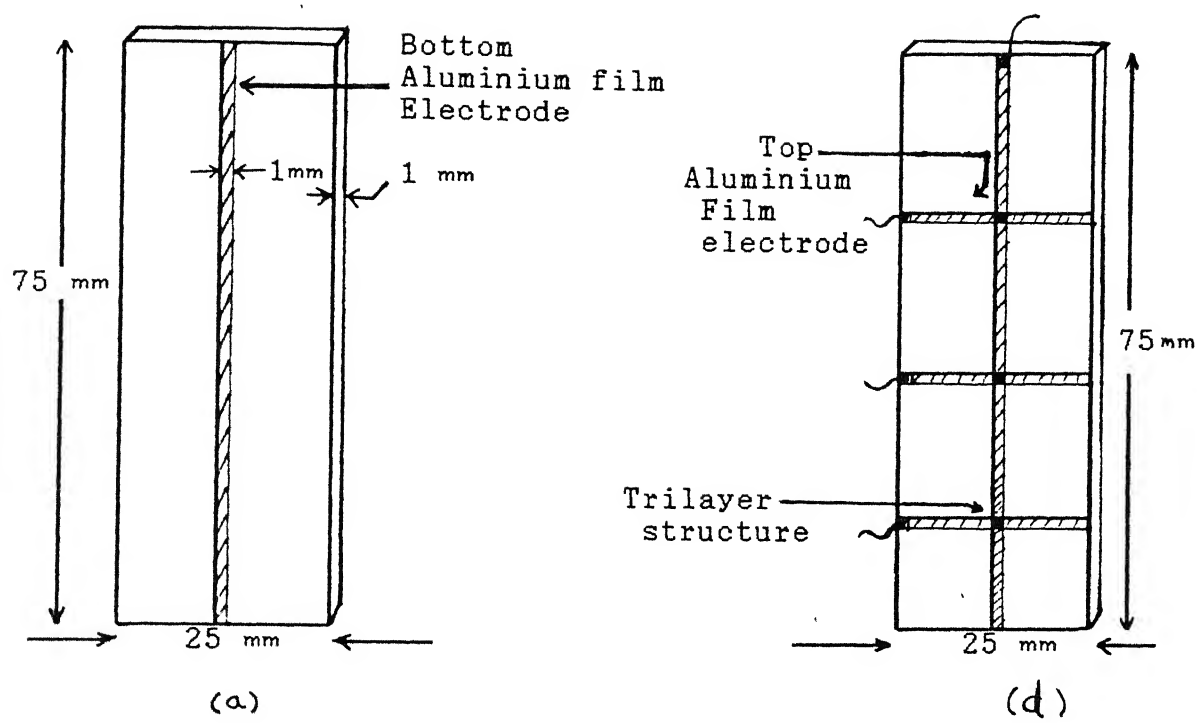

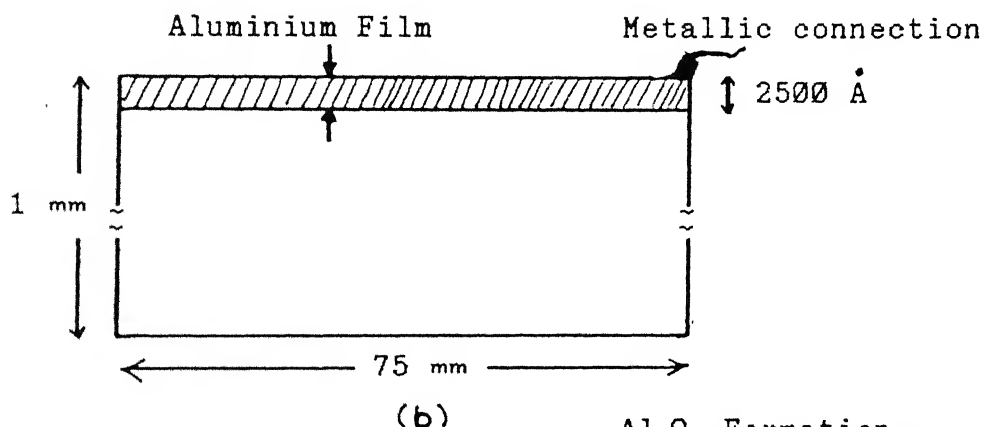

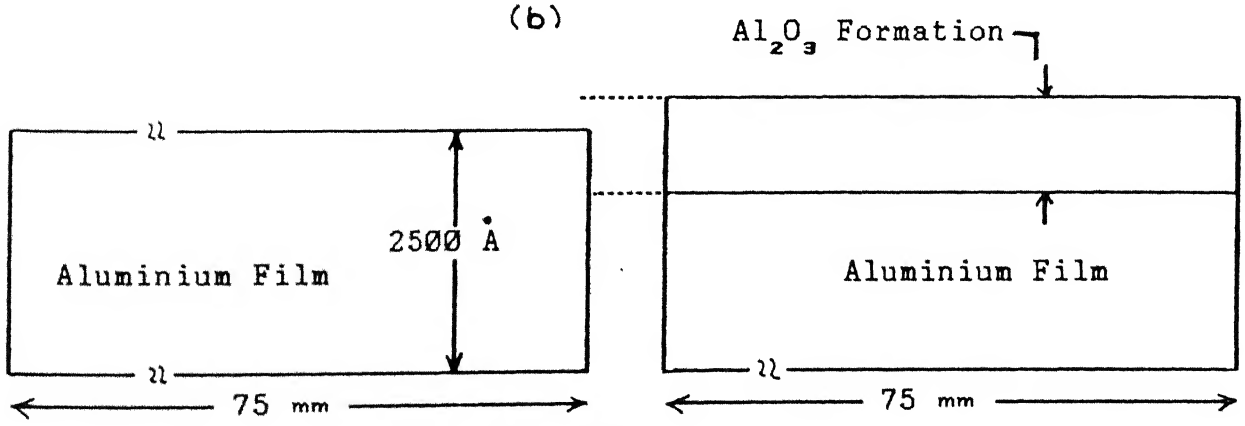

Fig 2.1 Different stages of preparation of Al-Al_2O_3-Al trilayer

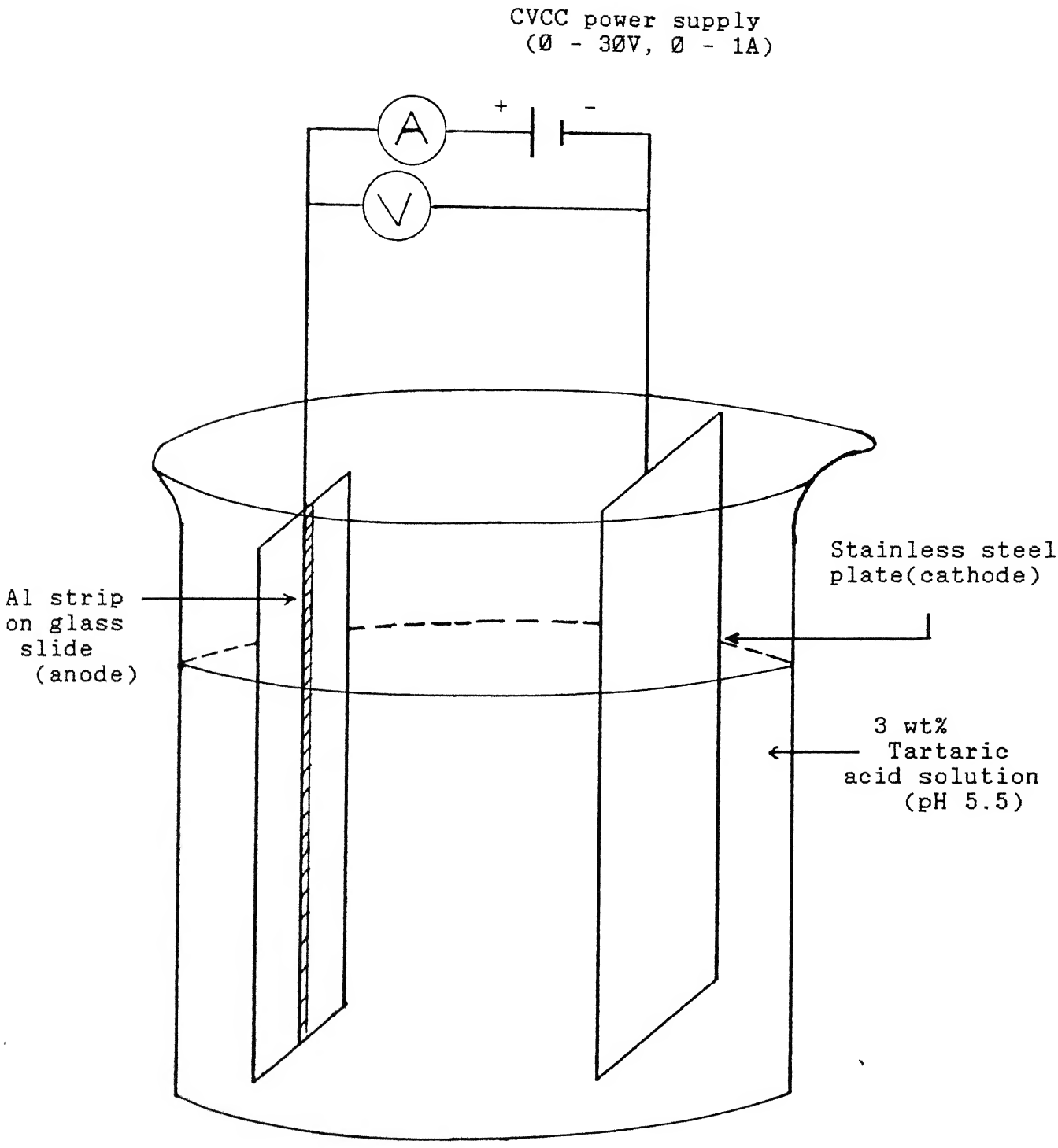

Fig 2.2 Schematic diagram of anodisation set-up.

2.2 CAPACITANCE MEASUREMENT

The capacitance measurements were carried out under ambient conditions, with a Hewllet Packard LCR Meter model HP4276A, at a frequency of 200 Hz and test voltage of 0.5V. The bottom electrode was always connected to the higher potential. These measurements were repeated after various interval of time lapsed to examine the effect of aging. The samples were transferred to a desiccator after each measurement, and held there for a specified period (1-12 days), at normal atmospheric pressure.

2.3 CURRENT VOLTAGE (I-V) MEASUREMENT

The electrical characteristics of all the samples were made by employing a set up shown in Fig 2.3. For this a Keithley Programmable voltage source (model 230) and a Keithley autoranging Picoammeter (model 495) were used. Sufficient time (1-2 minutes) was given to obtain the steady state current for recording each reading.

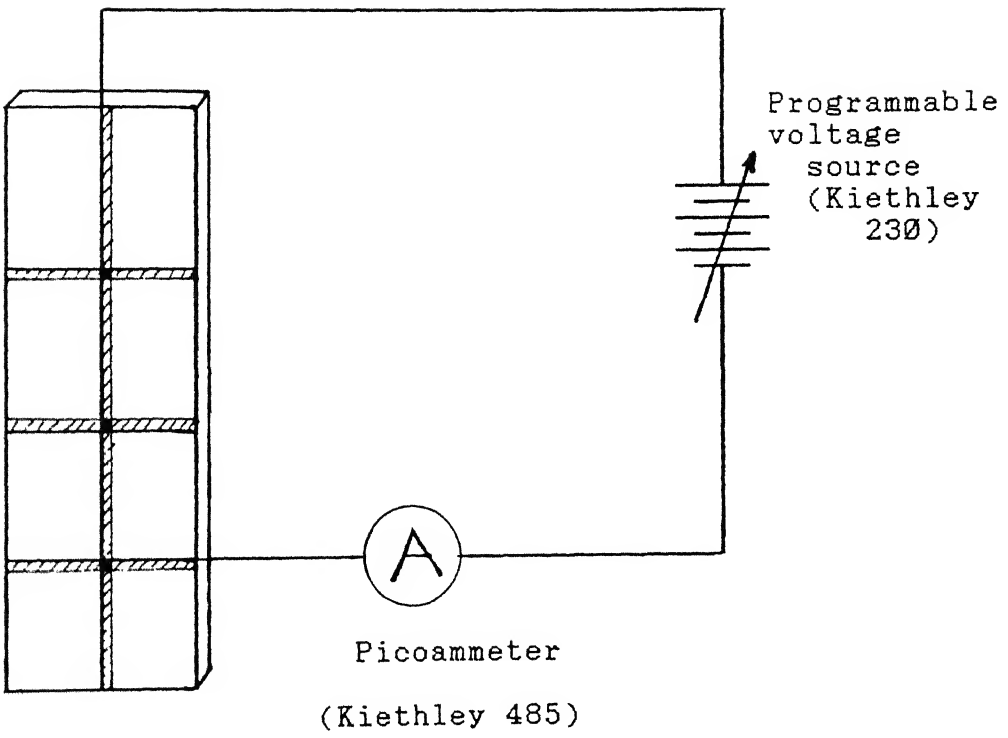

Fig 2.3 Schematic diagram of the experimental setup for current-voltage (I-V) meassurements.

3. RESULTS AND DISCUSSION

This chapter gives the description of the nature of the oxide layer formed on aluminium and the results and discussion of several experiments performed with the various $Al-Al_2O_3-Al$ sandwitches.

3.1 THE NATURE OF OXIDE

Like other metals, aluminium is unstable at room temperature. In contact with air/oxygen under ambient conditions it tends to form an oxide [40-43]. The initial oxide formation is very complex and involves a number of physical and chemical processes which are understood in terms of physical adsorption, chemisorption, absorption, etc. [43]. However, once the initial oxide layer is developed on the surface, further growth proceeds only if one (or both) of the species (namely, oxygen and metal atom) are able to pass through the oxide for reaction at either the oxide-metal or oxide-oxygen interface. The rate of further oxidation therefore depends not on the thermodynamics, but, on the kinetics of the reaction. Aluminium oxide is reasonably stoichiometric having a chemical composition (Al_2O_3) with low defect concentration. Generally, specific volume of the oxide is different from that of the metal consumed. The difference is best represented by the Pilling-Bedworth ratio (ϕ), defined as

$$\phi = \frac{\text{Molecular volume of oxide}}{\text{Atomic volume of metal}} = \frac{M_o\, d_m}{\eta^*\, M_m\, d_o}$$

where M_m is the atomic weight of the metal atom, M_o is the molecular weight of the oxide, η^* is the number of metal atoms per molecule of the oxide and d_m and d_o are the densities of the metal and the oxide, respectively. This ratio (ϕ) quantifies the protective ability of the oxide. If ϕ is less than unity, the oxide fails to cover the entire metal surface and forms discontinuous protective layer through which oxygen can readily pass. Thus, the rate of reaction is not affected by oxide growth. The amount of oxide formed depends only on the elapsed time at any given temperature. On the other hand, if ϕ is greater than unity, the oxide occupies larger volume than the metal and, in that case, it will be protective in nature. For oxidation of aluminium, the value of ϕ lies between 1.287 and 1.7 depending upon the type of Al_2O_3 formed. As a consequence, the growth occurs slowly after the initial oxide formation and stops eventually. Also, oxide layer is always under lateral compression and cause mechanical deformation, e.g. blistering occurs when adhesion of the oxide is weak and cohesion of oxide particles is strong; on the other hand, shear cracking takes place where adhesion is strong and cohesion is weak. Aluminium oxide formed by the thermal oxidation or anodization is amorphous in nature and transforms to γ-Al_2O_3 above 500°C. Also, the bonding is predominantly ionic, has large band gap and low leakage characteristics.

3.1.1 *Oxide formation*

Al_2O_3 was prepared by anodizing the aluminium film in an electrolytic cell containing 3 wt% tartaric acid solution of pH 5.5. The voltage applied (in the range of 2-20V) across the anode (aluminium film) and the cathode (stainless steel plate) causes current flow and, in turn, the dissociation of the electrolyte. This results in the release of oxygen ions which get attracted towards the anode. At anode, they react with aluminium and form a continuous thin film of Al_2O_3. The current initially is very high, but, decreases very rapidly (just after a few seconds) as the anodization proceeds. In fact, there is a continuous decrease in the field strength across the electrode with the growth of the oxide film. This causes fall in the ionic current which, in turn, decreases the rate of field drop. The rate of growth becomes so small within few tens of seconds that for all practical purposes the oxide thickness is said to have reached a limiting value. This is so because the electrolyte used (3 wt% tartaric acid solution of pH 5.5) does not have any solvent action on Al_2O_3. Therefore a continuous and uniform oxide layer results in the process [44]. The effective oxide thickness required to block the current flow varies linearly with the applied voltage. Once the barrier layer has been formed, an increase in the thickness could be done only by raising the applied voltage. For the 3 wt% tartaric acid electrolyte, having pH 5.5 (adjusted with NH_4OH), the limiting thickness of the barrier oxide is 13A / volt [40,41]. During anodization bubbles are observed on the cathode due to the hydrogen evolution. This helps in checking the

continuation of the reaction.

The oxide film obtained by anodization at 10 volts was separated out by dissolving the bottom aluminium layer in a solution of 8g mercuric chloride + 2 ml conc HCl +24 ml water and was transferred in succession to various petridishes filled with distilled water to ensure thorough cleaning and eventually taken on a copper grid for examination in a transmission electron microscope (TEM). The observation revealed that the film was continuous and pinhole free with no visible microstructure. Also, the diffused rings observed in the electron diffraction clearly indicated the amorphous nature of the aluminium oxide layer formed by anodization.

3.2 DIELECTRIC PROPERTIES

The capacitance of a bulk capacitor is given by

$$C_b = \varepsilon_o K A / d \qquad \ldots.(3.1)$$

where ε_o = permittivity of air K = dielectric constant of the insulator, A = cross section area of the capacitor formed, d = thickness of the dielectric Thus a plot of A/C_b versus d should be a straight line passing through the origin. Fig 3.1 shows A/C_b versus 'd' plots for alumina of different dielectric constants, viz. 9.6(Vaezi-Nizad [45]), 9.03(Hebard et.al. [19]), 8.51(Birey [5]), as found from expression 3.1. These clearly

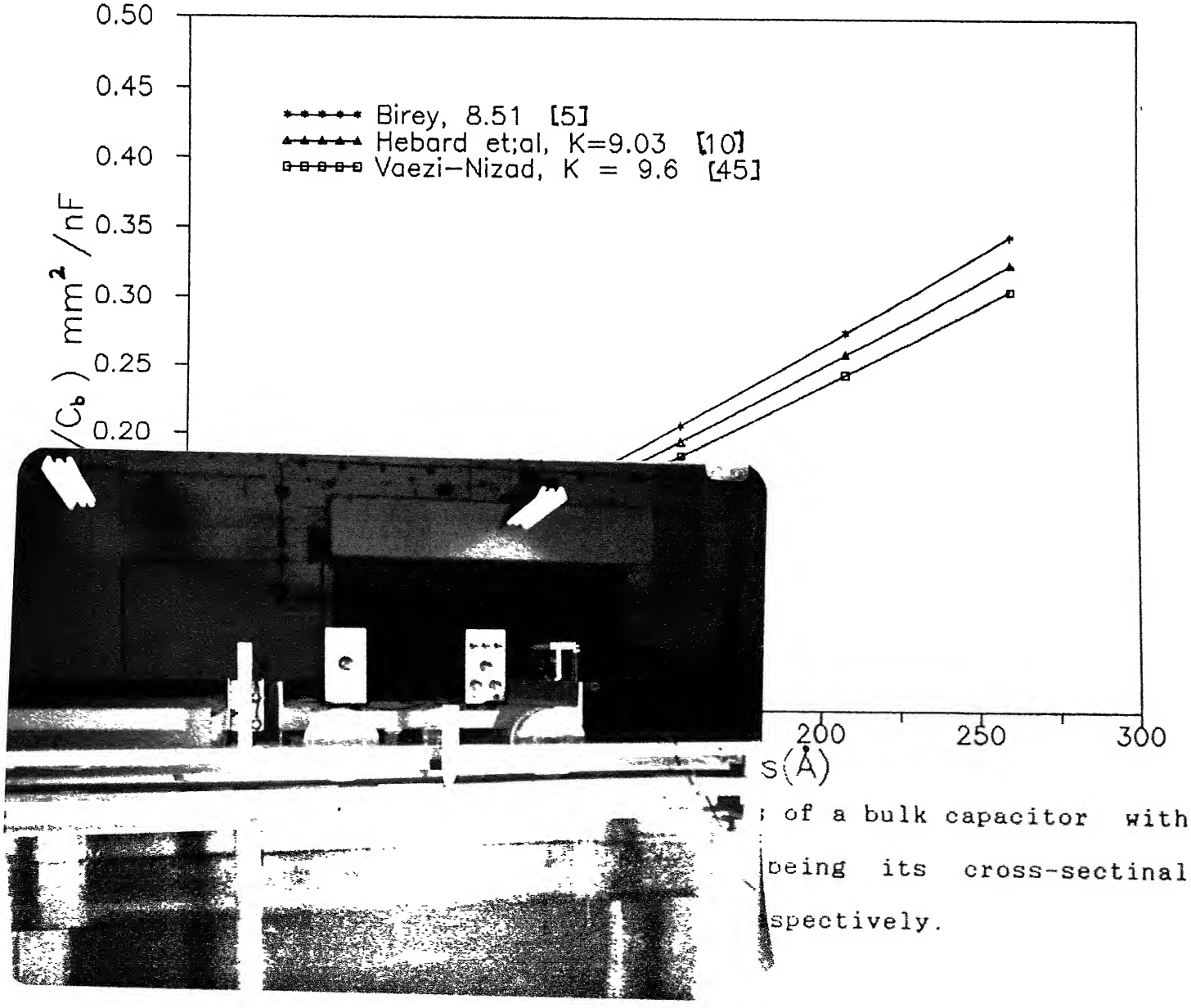

; of a bulk capacitor with
being its cross-sectinal
spectively.

depict (i) increase in the A/C_b with oxide thickness, and (ii) decrease of slope with the dielectric constant(K). Thus, in principle, the dielectric constant of an oxide can be determined from its capacitance measurement at a given thickness using expression 3.1 or from the slope of the A/C_b versus 'd' plot.

3.2.1 *Thickness dependence*

The measured capacitance C_m at 1ØØ Hz of the $Al-Al_2O_3-Al$ structure invariably decreases with oxide thickness (Fig 3.2). The decrease is, however, not smooth as the cross-sectional areas of various capacitors are different and ranges from Ø.7 to 1.Ø mm^2. Neverthless, the variation characteristics is similar to what is observed in cross-sectional surface area/volume ratio versus thickness curve (Fig 3.3). Clearly, the ratio increases sharply with decrease in thickness below 1ØØA. Since the measured capacitance also shows similar trends, it is believed that surface effects predominate below oxide thickness of 8ØA atleast(Fig 3.2).

Fig 3.4 shows A/C_m versus 'd' plot of various capacitors of oxide thickness in the range 26-26ØA. A least square fit of the data for straight line reveal the characteristic increase of A/C_m with thickness. However, the straight line does not pass through the origin as per expression 3.1, but makes an intercept on the y-axis. This observation suggests the existance of an additional constant, such that

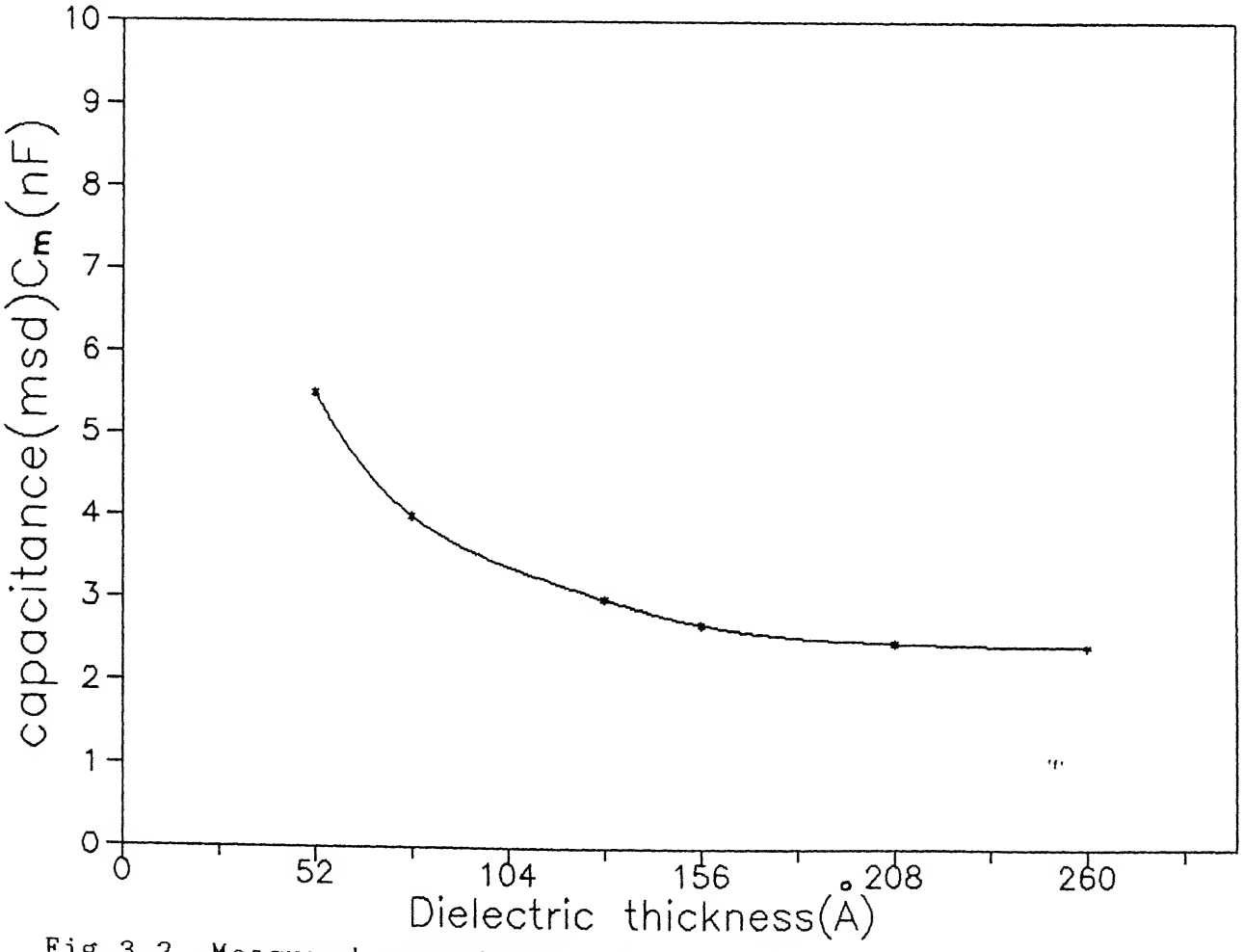

Fig.3.2 Measured capacitance (C_m) of the Al-Al_2O_3-Al structure as a function of insulator (Al_2O_3) thickness.

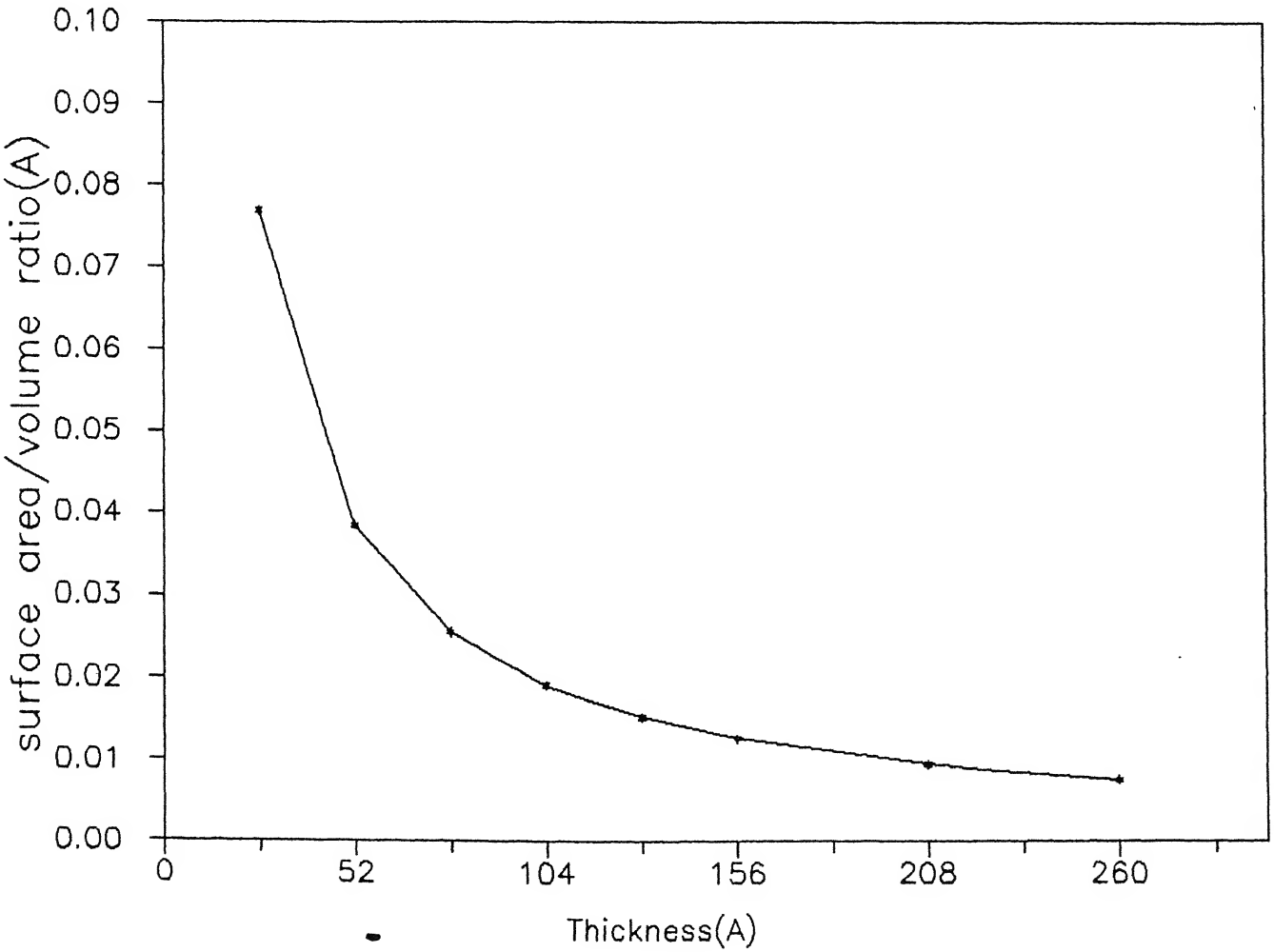

Fig.3.3 Variation of surface area / volume with thickness of the insulator.

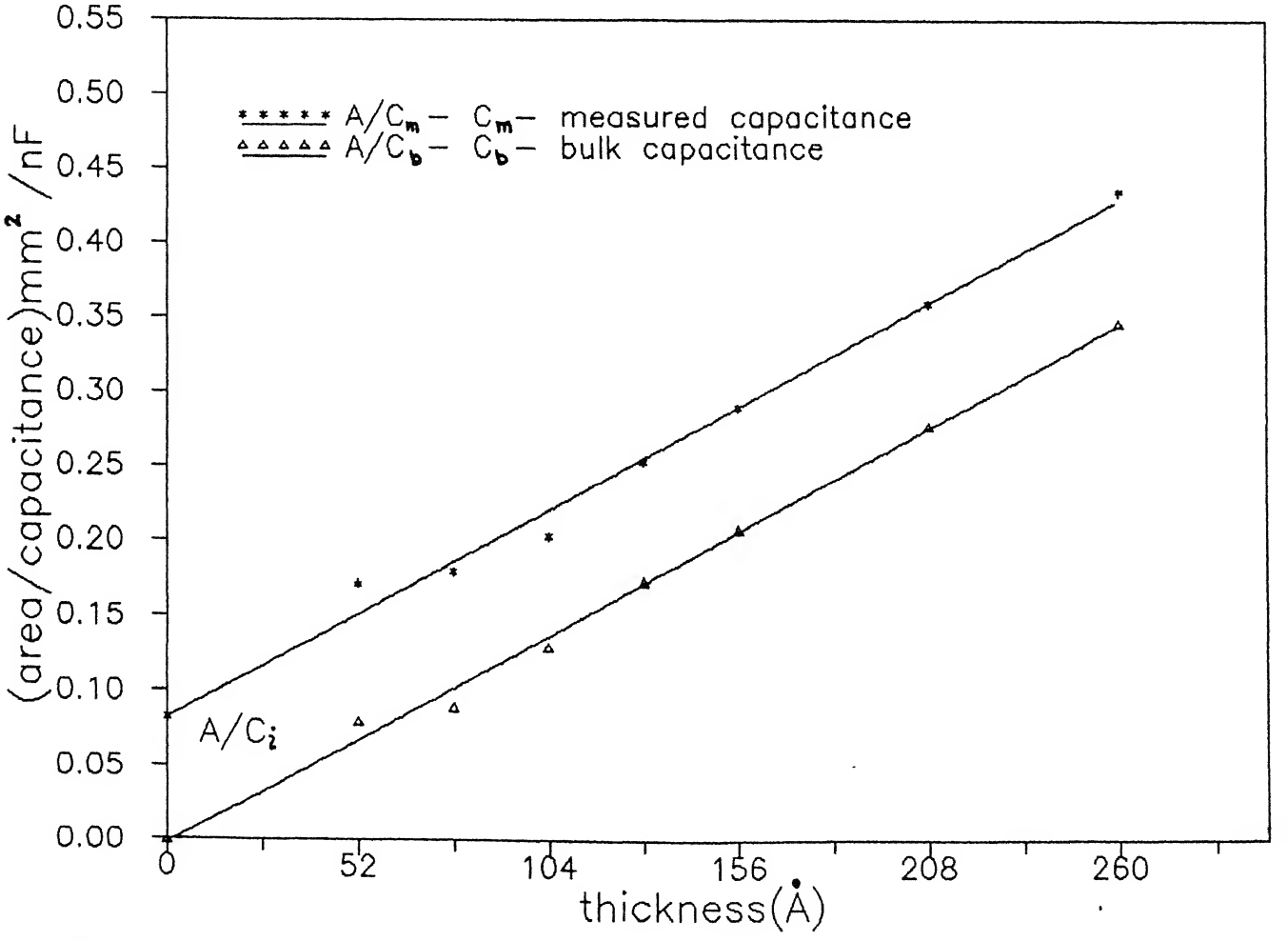

Fig.3.4 Variation of area/capacitance with thickness of Al-Al_2O_3-Al structure; A being cross-sectional surface area. C_i represents the interfacial capacitance = 1.22$\mu F/cm^2$.

$$A/C_m = B + d/(\varepsilon_o K) \qquad \ldots.(3.2)$$

where B is given by the intercept of A/C_m versus 'd' plot at the ordinate. As d $\rightarrow$ Ø, eq. 3.2 suggests that B can be thought of a term like A/C_i, where C_i is the capacitance associated with the interfaces. The situation is equivalent to two capacitors lying in series: (i) with capacitance of the bulk Al_2O_3, and (ii) having contribution arising from the interfaces. Thus, the net measured capacitance (C_m) can now be given by expression (1.3), viz.,

$$A/C_m = A/C_i + d/(\varepsilon_o K) \qquad \ldots.(3.3)$$

where the interfacial capacitance C_i is assumed to be proportional to area only. The value of the interfacial capacitance C_i, as found from the intercept (Fig 3.4) is 1.22 $\mu F/cm^2$ and corresponds to a capacitor of thickness ~ 62, 65 and 7ØA with dielectric constants 8.51, 9.Ø3, and 9.6, respectively. Since the bulk and the interfacial capacitance are in series, the measured value would be closer to the one having lower capacitance. Moreover, if the interfacial capacitance is considered to be constant, a stage may reach with increase in oxide thickness, when bulk capacitance becomes equal to the interfacial capacitance (Notice that bulk capacitance decreases with increase in the oxide thickness, expression 3.1) and even smaller at higher thicknesses. In the later case, one would eventually measure the bulk capacitance when its value reaches about one hundredth of C_i. The bulk contribution (C_b) can be determined at each oxide thickness from

expression 3.3 by substracting the interfacial component (A/C_i) from the measured (A/C_m) values. Fig 3.5 shows the variation of C_b with oxide thickness for a cross-sectional area of 1.74 mm^2. Also, it depicts the oxide thickness at which interfacial and bulk capacitance values become equal. The value of the equivalent oxide thickness being 75A. As the oxide thickness increases beyond this value, the total measured capacitance (C_m) gradually approaches the bulk capacitance value (C_b). The estimated C_b follows expression 3.1. This is demonstrated by A/C_b versus 'd' plot (Fig 3.6 and also 3.4) clearly, i.e. - straight line passing through origin.

The slope of the straight line (Fig 3.4) gives the value of the dielectric constant (K) as 8.5, which is somewhat smaller than 9.6 and 9.Ø3 found by Vaezi-Nizad [45] and Hebard et.al. [19], respectively, but is close to 8.51, obtained by Birey [5].

The Al_2O_3 films formed by anodization are hydrated. They are also under stress and may contain water molecules, aluminium ions, ingredients of electrolyte, etc. [48]. Therefore, to remove the moisture (if any) and relieve the stress, the anodized films were heated in air at 16Ø°C for 4 hours before depositing the top aluminium electrode. The capacitance measurements of the resulting Al-Al_2O_3-Al structures indeed show increase in A/C_m values with oxide thickness (Fig 3.7). The straight line obtained by least square fitting of the data gives intercept at the ordinate. This once again points out the existence of the interfacial contribution to the total capacitance. The interfacial

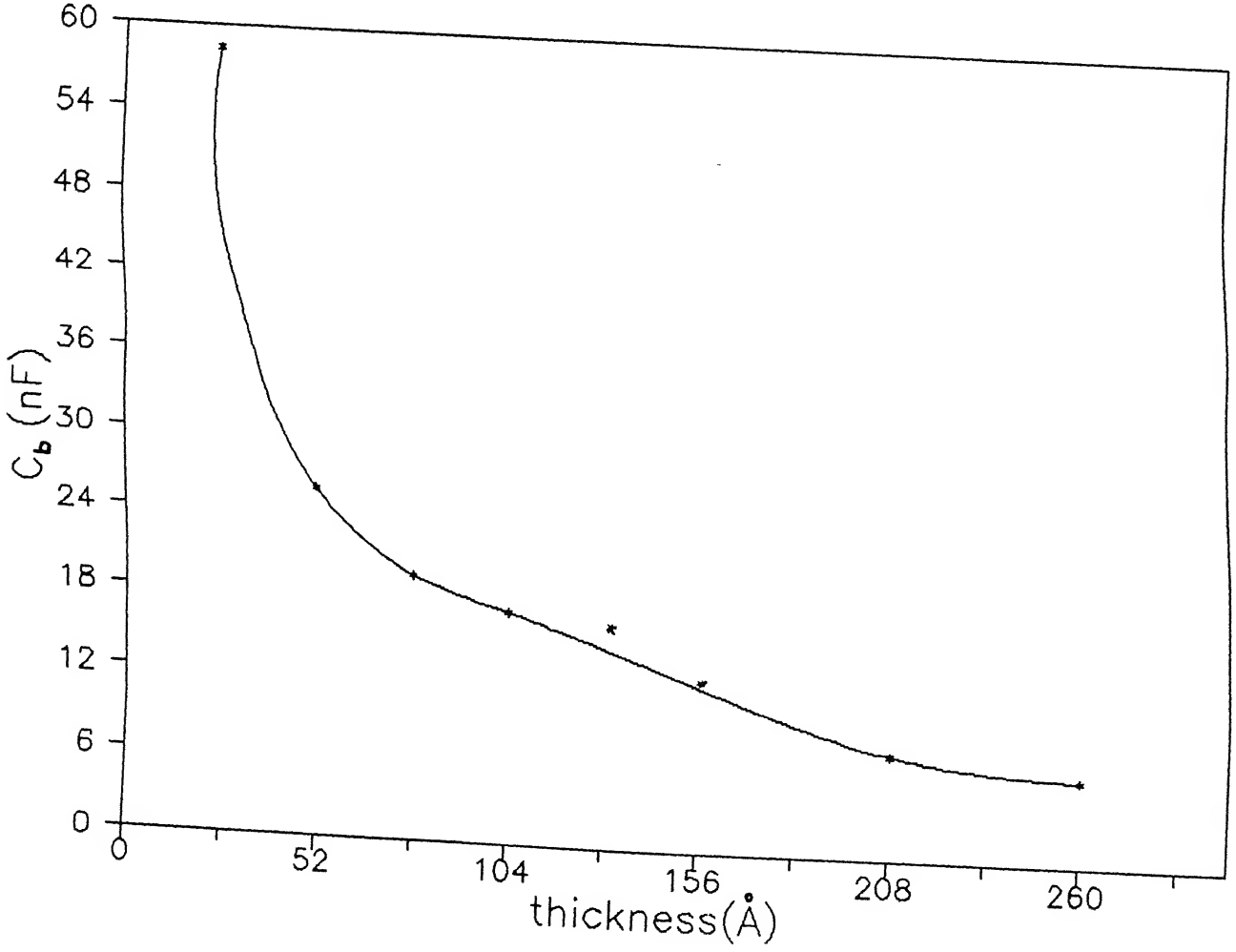

Fig.3.5 Variation of bulk capacitance (C_b) with oxide thickness in Al-Al_2O_3-Al structure. The cross-sectional area being 1.74 mm^2.

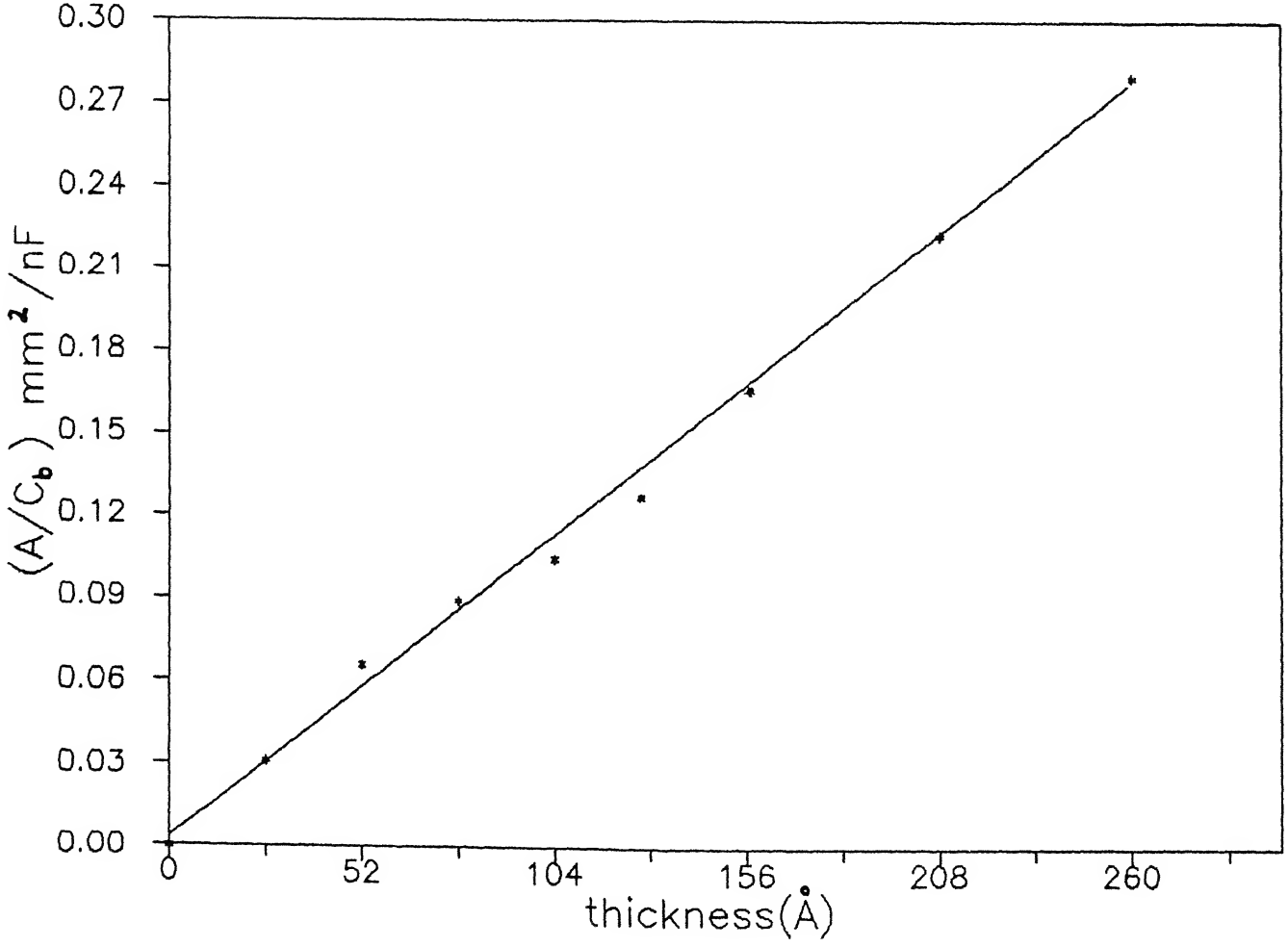

Fig.3.6 Variation of area/capacitance (A/C_b) with oxide thickness in $Al-Al_2O_3-Al$ structure ; A being cross-sectional surface area and C_b the bulk capacitance.

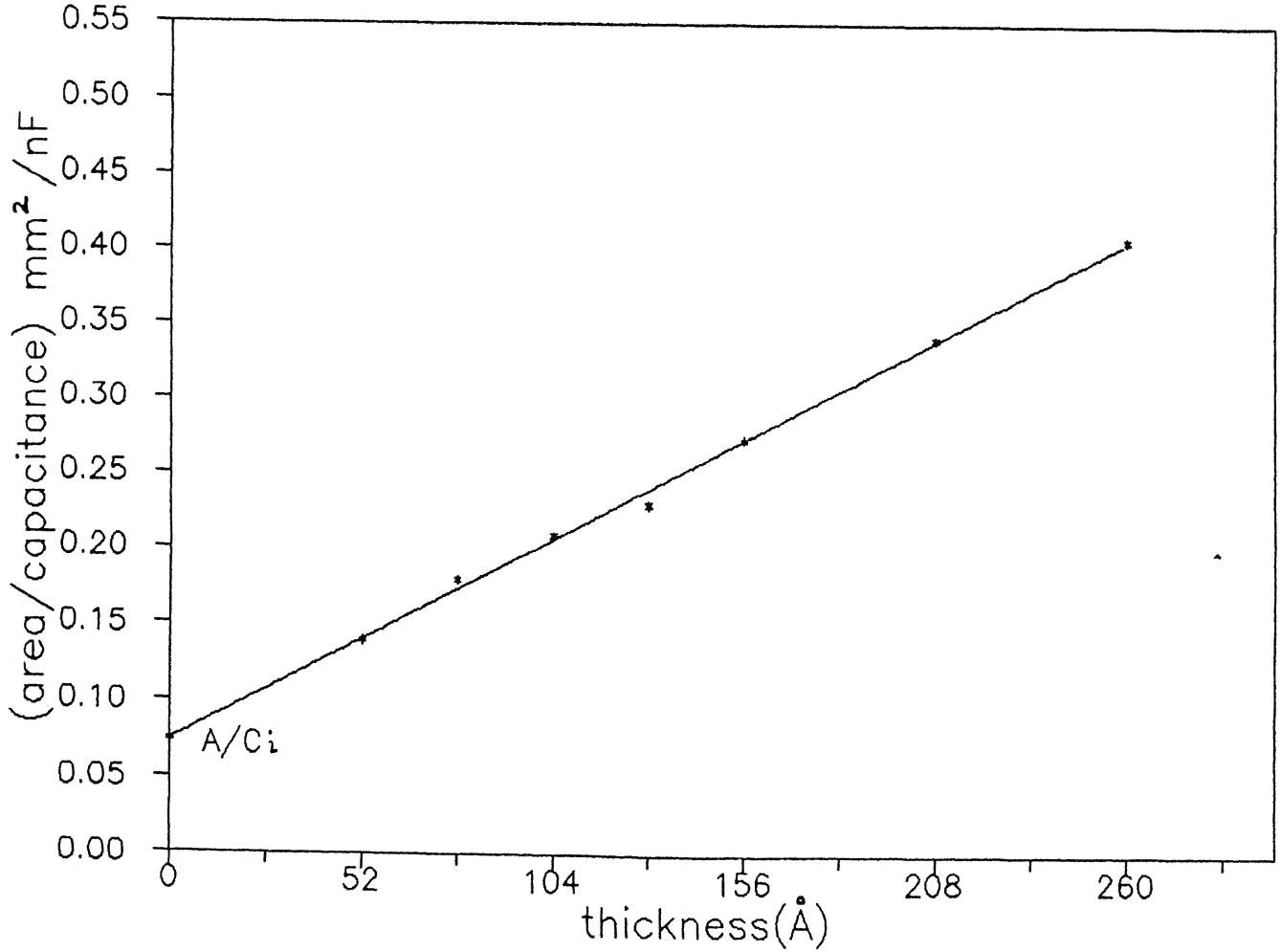

Fig.3.7 Variation of area/capacitance with thickness of $Al-Al_2O_3-Al$ structure (which is formed after heating the anodized film at 160°C for 4 hrs in air); A being the cross-sectional surface area. C_i is the interfacial capacitance.

capacitance (C_i) value turns out to be 1.36 $\mu F/cm^2$.

When the two A/C_m versus `d ´plots of different sets of samples (one made just after anodization and the other after heating the anodized Al_2O_3 films in air at 160°C for four hours) are compared (Fig 3.8), a slight change (decrease) in slope is observed in the heated samples. This means that the dielectric constant increases with annealing. The value now becomes 9.0. This suggests that the dielectric quality of Al_2O_3 is improving on annealing. Moreover, the straight line shifts downwards indicating an overall increase in the value of the capacitance and hence the storage capacity. Also, the interfacial capacitance has increased somewhat, i.e. from 1.22 to 1.36 $\mu F/cm^2$. When the samples were heated at 200°C instead of 160°C, as mentioned above, the dielectric constant further increased to 10.9.

3.2.2 *Area effect*

In order to study the effect of the junction area on the capacitance, samples of nearly same cross-sectional area of 1 mm^2 and 1.96 mm^2, were fabricated with oxide thickness in the range of 26-260A. In this case, the anodized films were annealed in air at 200°C for 4 hours. The plots of measured capacitance (C_m) versus thickness (d) for two sets of samples are given in Fig 3.9. Table 3.1 summarises actual areas and the corresponding capacitance (C_m) values. These results reveal that the capacitance value increases in proportion to area for thickness greater than 50A atleast. One can, therefore, say that capacitance of thin alumina films indeed

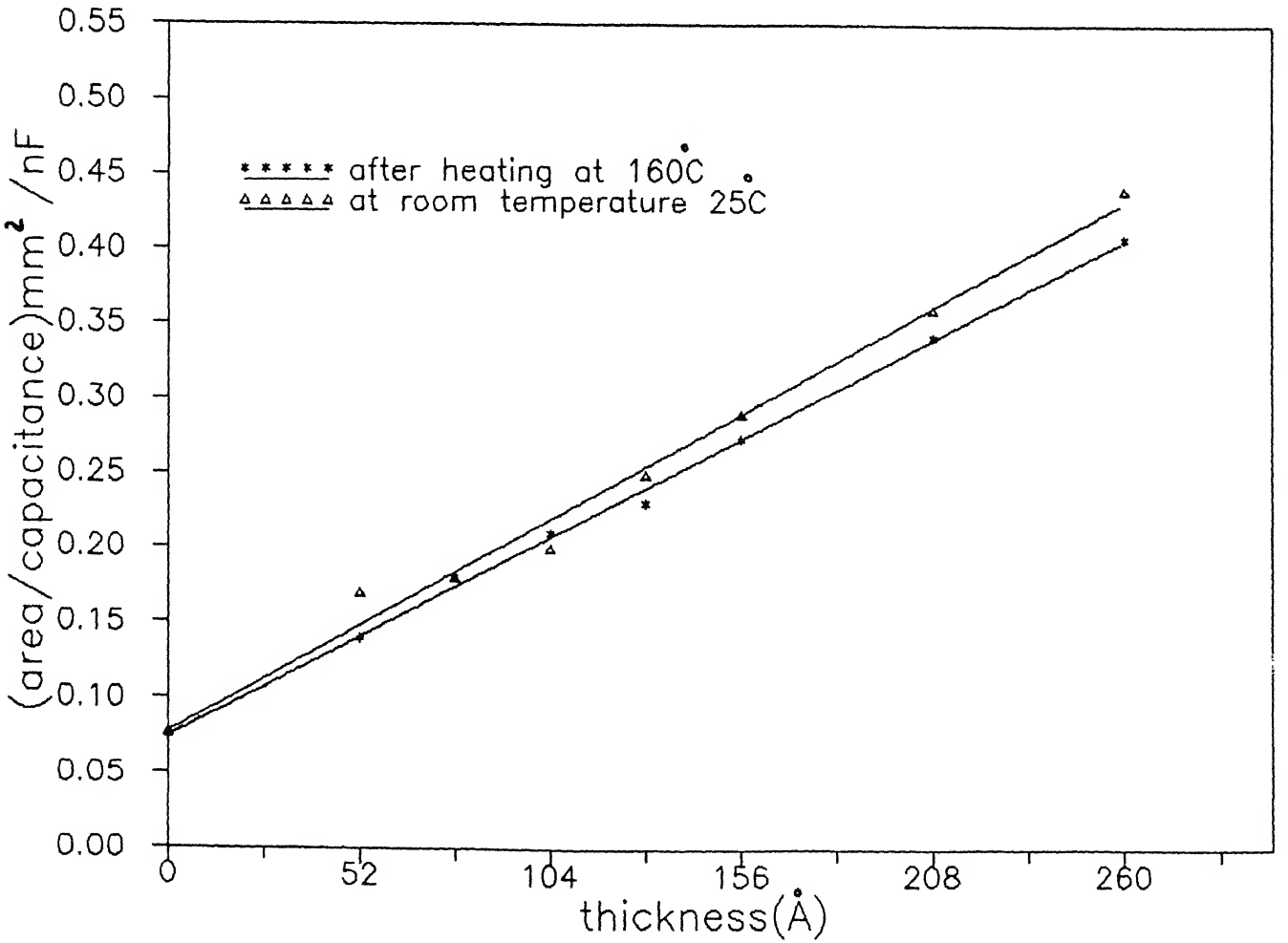

Fig.3.8 Variation of area/capacitance with thickness of two Al-Al_2O_3-Al structures; one anodized and made at room temperature and other formed after heating the anodized film at 160°C for 4 hrs in air.

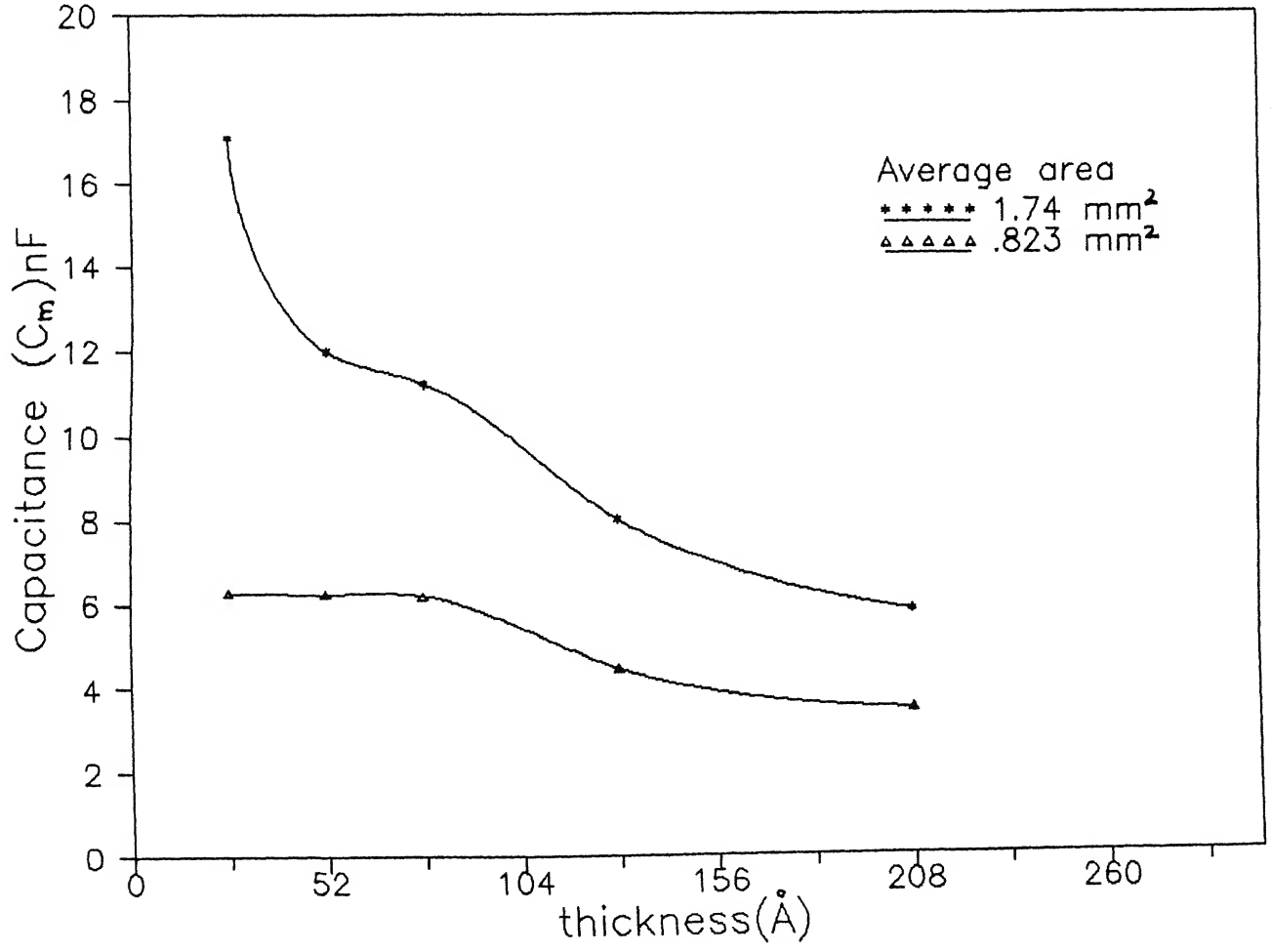

Fig.3.9 Measured capacitance (C_m)of Al-Al_2O_3-Al structure as a function of oxide thickness for two cross-sectional areas.

TABLE 3.1 MEASURED CAPACITANCE C_m AS AS A FUNCTION OF OXIDE THICKNESS

Thickness (A)	Total Capacitance of Al-Al_2O_3-Al (nF)			
	For area ~ Ø.83 mm^2		For area ~ 1.74 mm^2	
	Actual area mm^2	C_m(nF)	Actual area mm^2	C_m(nF)
26	Ø.718	6.3	1.81	17.1
52	Ø.92Ø	6.25	1.7Ø	12.Ø
78	Ø.896	6.2Ø	1.71	11.24
13Ø	Ø.848	4.44	1.95	1Ø.7Ø
156	Ø.814	3.54	1.7Ø	7.16
2Ø8	Ø.988	3.47	1.72	5.8Ø

vary in the same manner with area as in bulk i.e. capacitance is directly proportional to area. Moreover, the values of the interfacial capacitance found from the intercept of A/C_m versus 'd' plot at the ordinate show similar dependence on area. Fig 3.1Ø depicts this behaviour quite clearly not only for fresh structures but also for aged ones. The effect of aging is discussed separately in the Section 3.2.3 below. The above observation indicates that even the interfacial capacitance is directly proportional to area and justifies the relation (3.3).

3.2.3 *Effect of aging*

The stability of the trilayered capacitors with time was studied by measuring their capacitances after 1, 2, 3, 4, 5, and 12 days, rsepectively. Fig 3.11 shows the measured capacitance (C_m) for samples of oxide thickness 26, 13Ø and 2Ø8A. In all the cases, the capacitance (C_m) decreases fast initially, but, tends to assume a constant value with time. Also, the extent of decrease is more at lower oxide thicknesses. Even the interfacial capacitance (C_i) is found to decrease and stabilize with time. These results are indicative of some changes taking place in the bulk, as well as at the interfaces. One possible reason for this is the increase in the thickness of the film with time due to the neutralization of the positively charged aluminium ions and/or the capturing of the electrons by deep lying ionized donors [5,48]. The increased thickness of the Al_2O_3 can be estimated from the capacitance (C_m) data obtained after ten days of aging. For this,

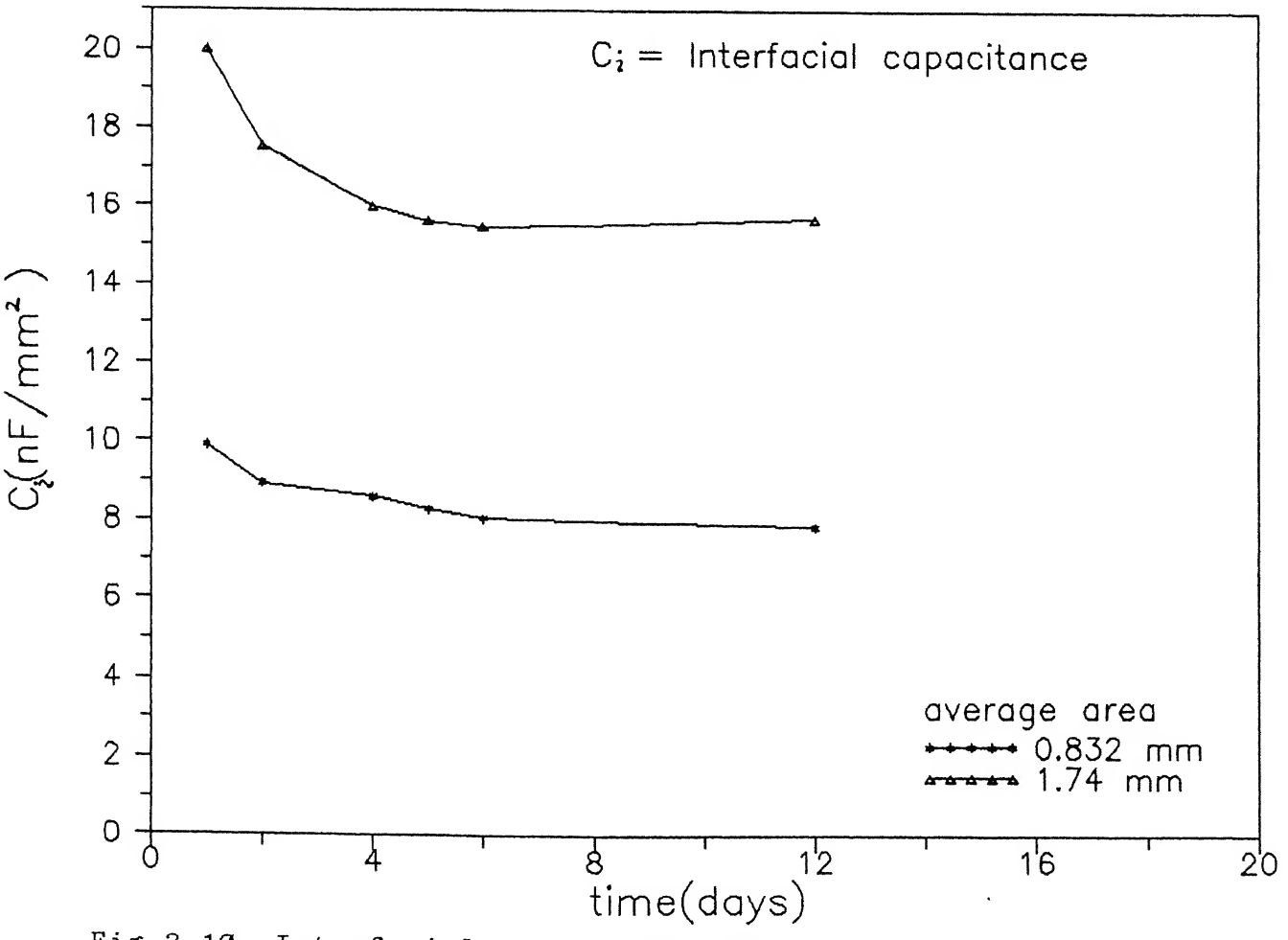

Fig.3.1Ø Interfacial capacitance (C_i) of Al-Al_2O_3-Al structures (formed after heating the anodized film at 2ØØ°C for 4 hrs in air) as a function of time for cross-sectional areas Ø.83mm² and 1.74mm².

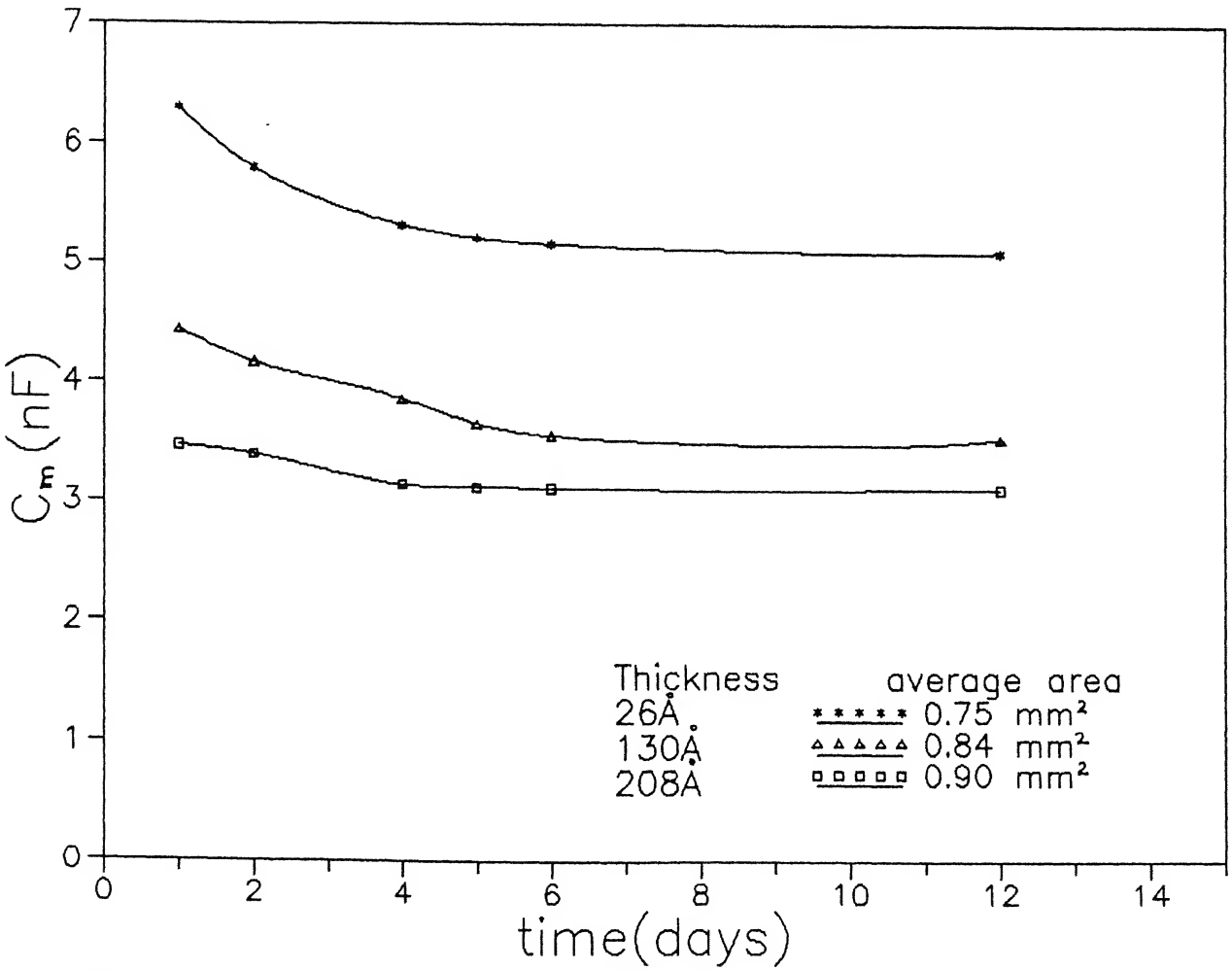

Fig.3.11 Measured capacitance (C_m) of Al-Al_2O_3-Al structures (formed after heating the anodized film at 200°C for 4 hrs in air) as a function of time for three different thicknesses.

the bulk capacitance (C_b) values are derived by subtracting the interfacial component (as mentioned in section 3.2.2). These can be taken to evaluate dielectric thickness using eq.3.1. Fig 3 12 shows the increased thickness against the initial Al_2O_3 thickness. It clearly reveals that the extent of increase is progressively becoming more with oxide thickness. Such a result, infact, provides support for the belief of increase in bulk thickness of Al_2O_3 with time. The exact mechanism for such a phenomemenon cannot however be spelt out with the limited information available.

3.3 - CURRENT-VOLTAGE CHARACTERISTICS

3.3.1 *Conduction process(es)*

The J-V characteristics of Al-Al_2O_3-Al trilayer structures fabricated in the manner described in section 2.1 with insulator thickness 78, 130, 156, 208 and 260A, obtained by maintaining the bottom electrode as positive are shown in fig(3.13). Two types of regions are invariably observed :

(i) A linear region with marginal increase in current with the increase in the voltage .

(ii) A non-linear region with steep rise in current by a few orders of magnitude with increase in voltage beyond a threshold.

Since the dielectric (Al_2O_3) films used are of less than 300 A thick, a potential as low as few volts induces a field of the

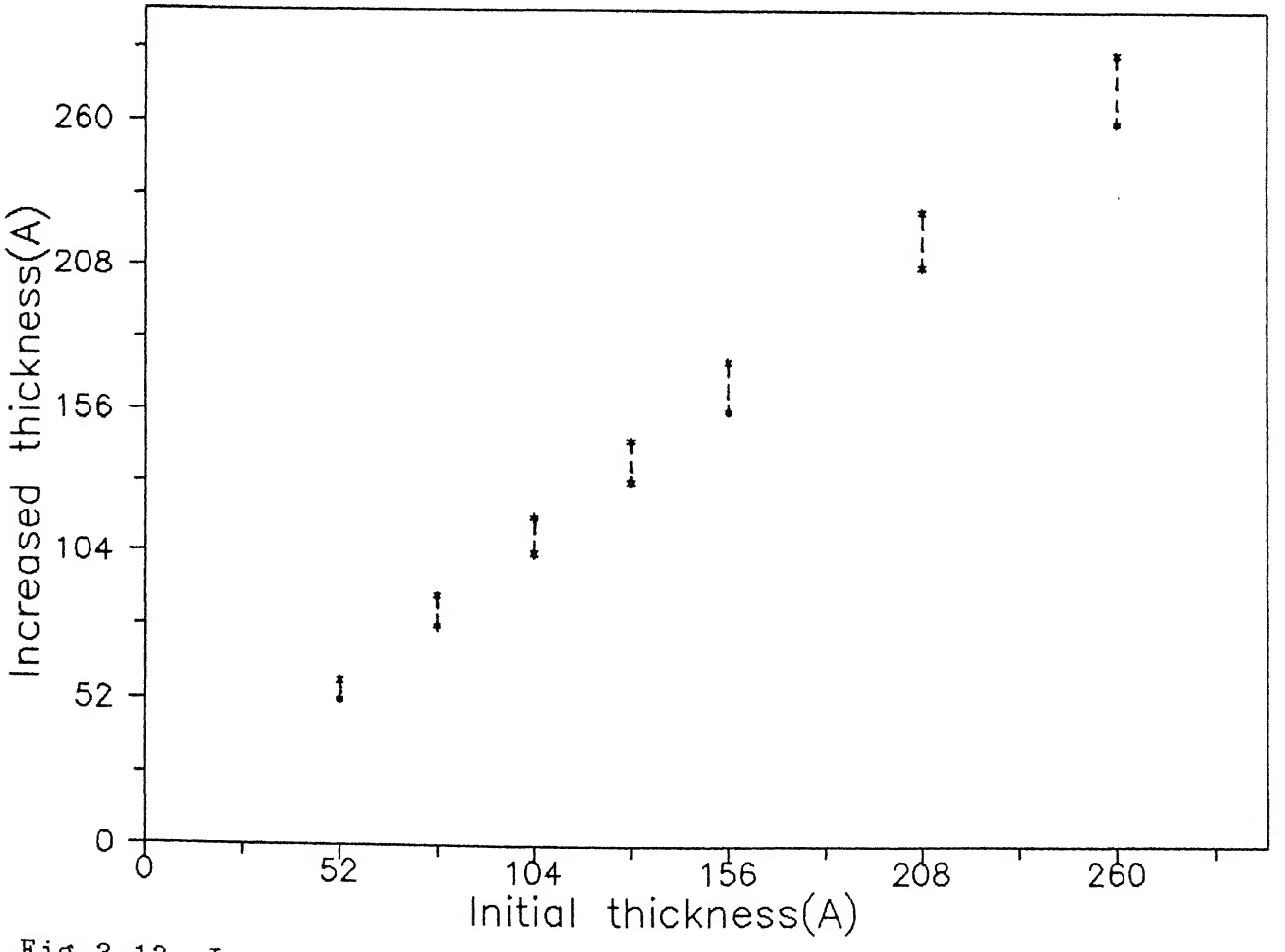

Fig.3.12 Increased thickness of Al_2O_3 after ten days of aging.

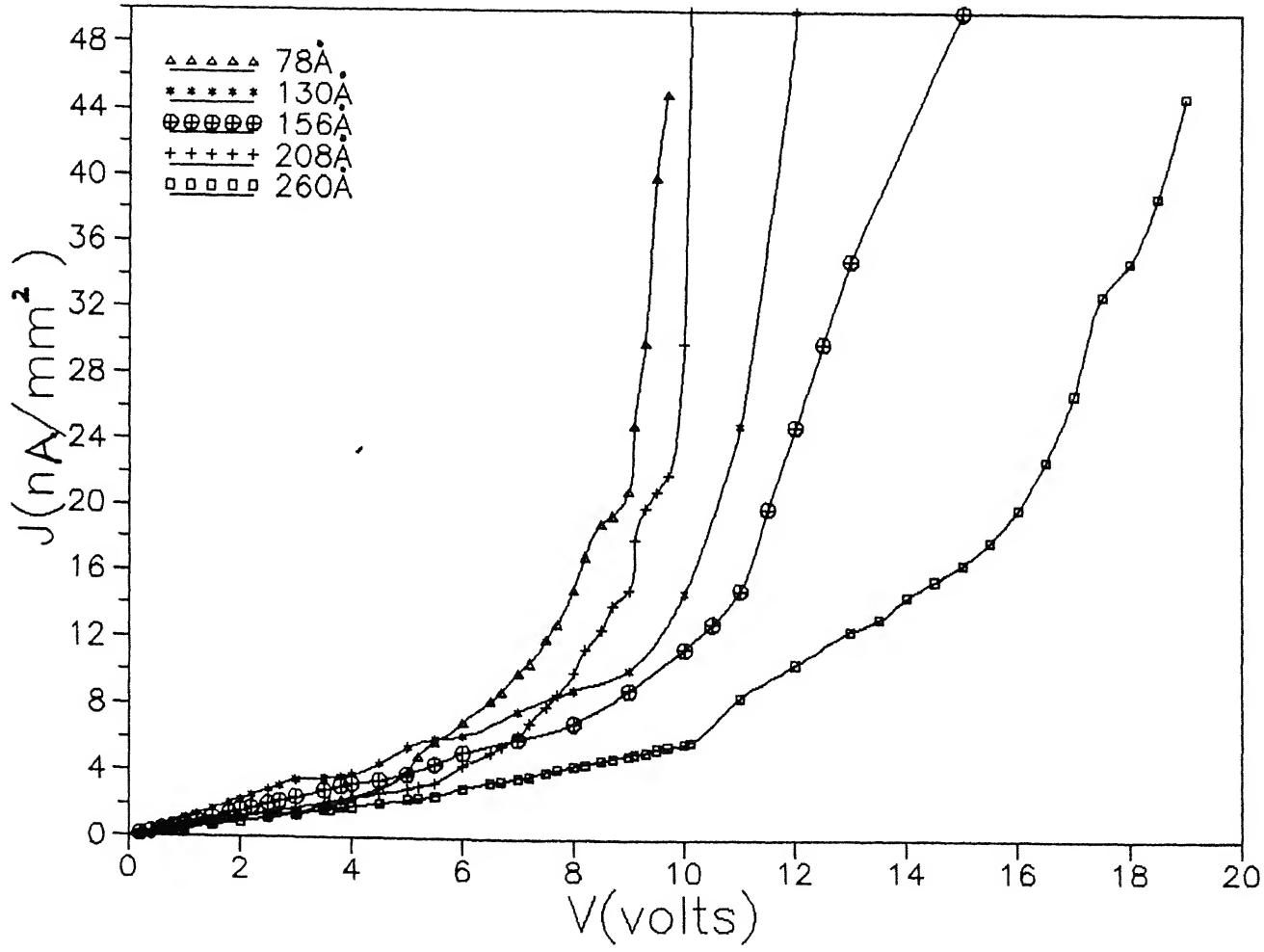

Fig.3.13 Current density (J) versus voltage (V) characteristics of $Al-Al_2O_3-Al$ structures for various oxide thicknesses.

order of 10^6 V/cm across them. This means that the present studies correspond primarily to high electric field situations where a number of conduction processes get involved in transporting the electric charge [27]. The most prominent of these are ohmic, tunneling, Schottky-emission, Poole-Frenkel effect and field-emmission (Section 1.2). By analyzing the observed experimental data in depth, the range of operation of a given conduction process could be identified (Table 3.2).

All the J-V plots depict a linear behaviour upto a particular voltage, beyond which the current is non-linear with the voltage. The linear portion in the low voltage regime indicates the ohmic conduction through aluminium oxide. The current density (J) is of the order of 10^{-13} A/cm^2. This (J) value is many orders of magnitude higher than expected from the carrier generation in bulk alumina. The source of increased current density is believed to be the inherent defect nature of thin films, e.g., high donor density (due to free metal atoms present), traps, stresses, impurities, etc. Table 3.3 gives the threshold voltages as a function of oxide thickness. The results clearly reveal an increase in the threshold voltage with the oxide thickness. The inverse of slope of the linear part in the J-V plot gives V/J, called the tunnel resistivity. Fig 3.14 shows the variation of (V/J) or resistance (Ω/cm^2) as a function of oxide thickness. This result is consistent with the prediction of Simmons [28] for all except the lowest oxide thickness ~ 50A.

TABLE 3.2 CHARACTERISTICS OF VARIOUS CONDUCTION MODES FOR THIN INSULATING FILMS

Conduction	Plot	Nature	Remarks
Ohmic	J vs V	Straight line	at very low voltages
Schottky Emission	ln J vs $V^{1/2}$ or ln J/V^2 vs $1/V$	Straight line with positive slope Curve with a definite minimum	Richardson Schottk equation with slope giving β_s (field lowering coefficient Modified Schottky equation
Poole Frenkel Effect	ln J vs V or ln J/V vs $V^{1/2}$	Straight line with positive slope Straight line and Horizontal	Richardson Sochttky equation with slop giving $\beta_{p!}$ (field lowering coefficient Poole-Frenkel current expression
Tunneling	ln J/V^2 vs 1/V	Straight line with negative slope	Fowler Nordheim Tunneling Equation

Richardson-Schottky equation: $J = B \exp(B' * V)$ [33]

B, B′ are constants

Fowler-Nordheim equation : $J = A V^2 \exp(-A'/V)$ [3Ø]

A, A′ are constants

Poole-Frenkel equation: $J = C V \exp(C' * V)$ [36]

C,C′ are constants

Modified Form (Schottky) : $\ln J/V^2 = B'' \sqrt{V} + 2\ln(1/V)$

B'' is a constant

TABLE 3.3 THRESHOLD VOLTAGES OF Al-Al_2O_3-Al STRUCTURES

Anodisation voltage (volts)	Oxide Thickness (Å)	Threshold voltages from J -V plots (volts)	Voltage from the minimum in $\ln J/V^2$ vs V^{-1} plot (volts)
6	78	4	4.5Ø
1Ø	13Ø	6.5	8.2Ø
12	156	8.Ø5	8.16
16	2Ø8	8.6	7.ØØ
2Ø	26Ø	1Ø.Ø	1Ø.6Ø

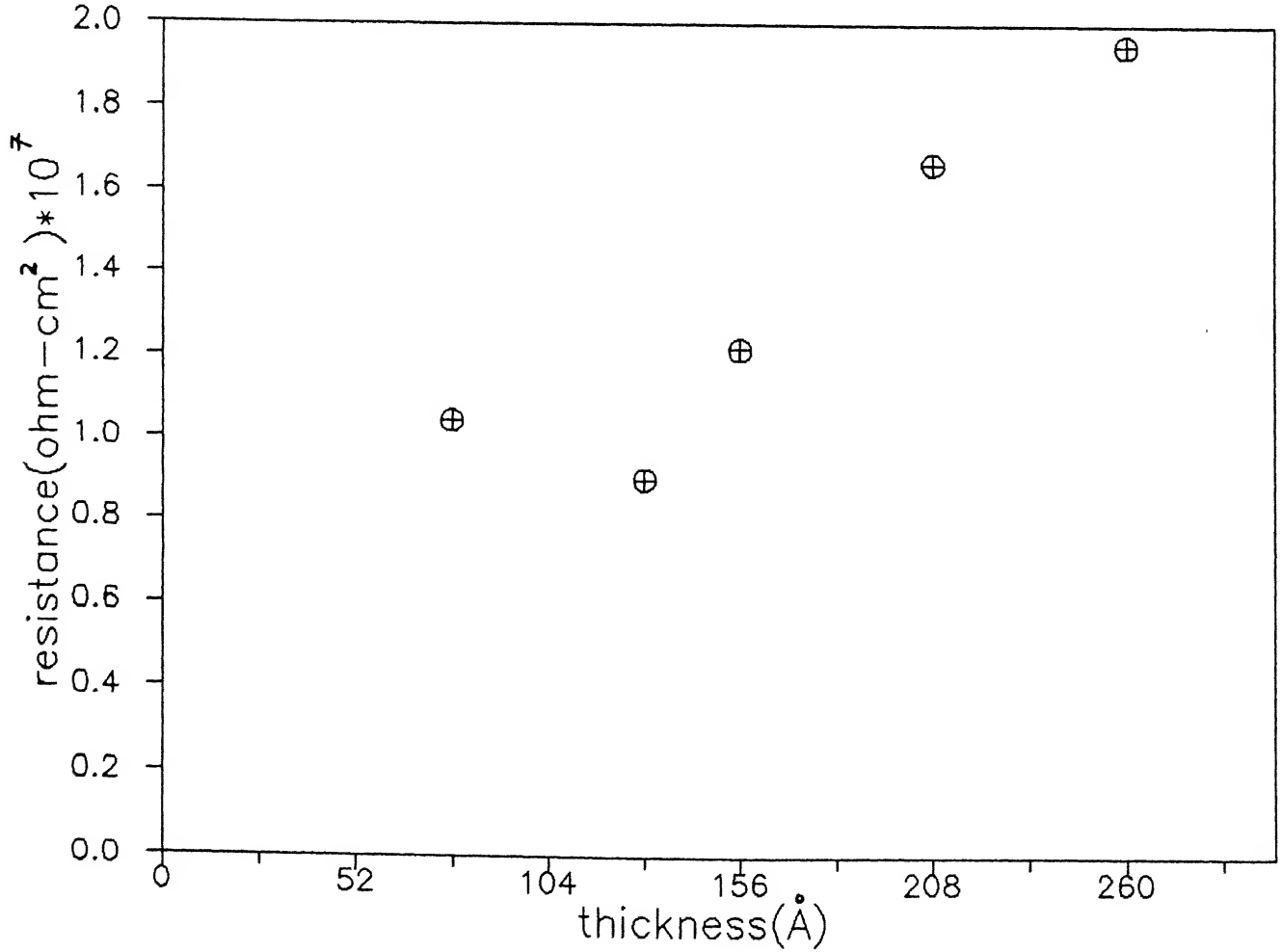

Fig.3.14 Variation of resistance (Ω-cm^2) with thickness of $Al-Al_2O_3-Al$ structures for various oxide thicknesses.

In order to identify the mechanism(s) of conduction operating, it is necessary to represent the current density (J)-voltage (V) characteristics in proper form. As, for example, the plots of ln J versus $V^{1/2}$ gives an idea about the regime of Schottky emission. The equation (1.13) requires that if the Schottky emission indeed occurs ln J versus $V^{1/2}$ plot should exhibit linear characteristics. The plots given Fig(3.15) do show linearity though in a small voltage range only. The non linearity present in low voltage regime indicates the transition from the ohmic behaviour to Schottky emission. In the higher voltage regime, the deviation from linearity is possibly due to the participation of another conduction mechanism involving high electric fields. Difficulties, however, arises with this interpretation as the current density dependence of the type $\ln J \propto V^{1/2}$ is attributed to either the Schottky-emmision or Poole-Frenkel effect (eq. 1.13). Therefore, in-depth analysis is required of the data to ascertain conclusively which of the above effects is involved. To find an answer, ln (J/V) versus $V^{1/2}$ plots are also made. When both the plots namely ln J versus $V^{1/2}$ and ln (J/V) versus $V^{1/2}$, show straight lines in the same voltage regime, Poole-Frenkel effect or bulk-limited process is said to be applicable. If only ln (J/V) versus $V^{1/2}$ gives a straight line, Schottky-emission or electrode limited process is operative. Thus careful analysis of ln J versus $V^{1/2}$ and ln (J/V) versus $V^{1/2}$ plots (fig 3.15 & 3.16) bring out cleraly the voltage regimes of Schottky-emission and Poole-Frenkel effects. The findings are summarized in Table 3.4. It is worth noting that ln (J/V) versus $V^{1/2}$ plots shows distinctly the ohmic conduction regime by horizontal lines (Fig

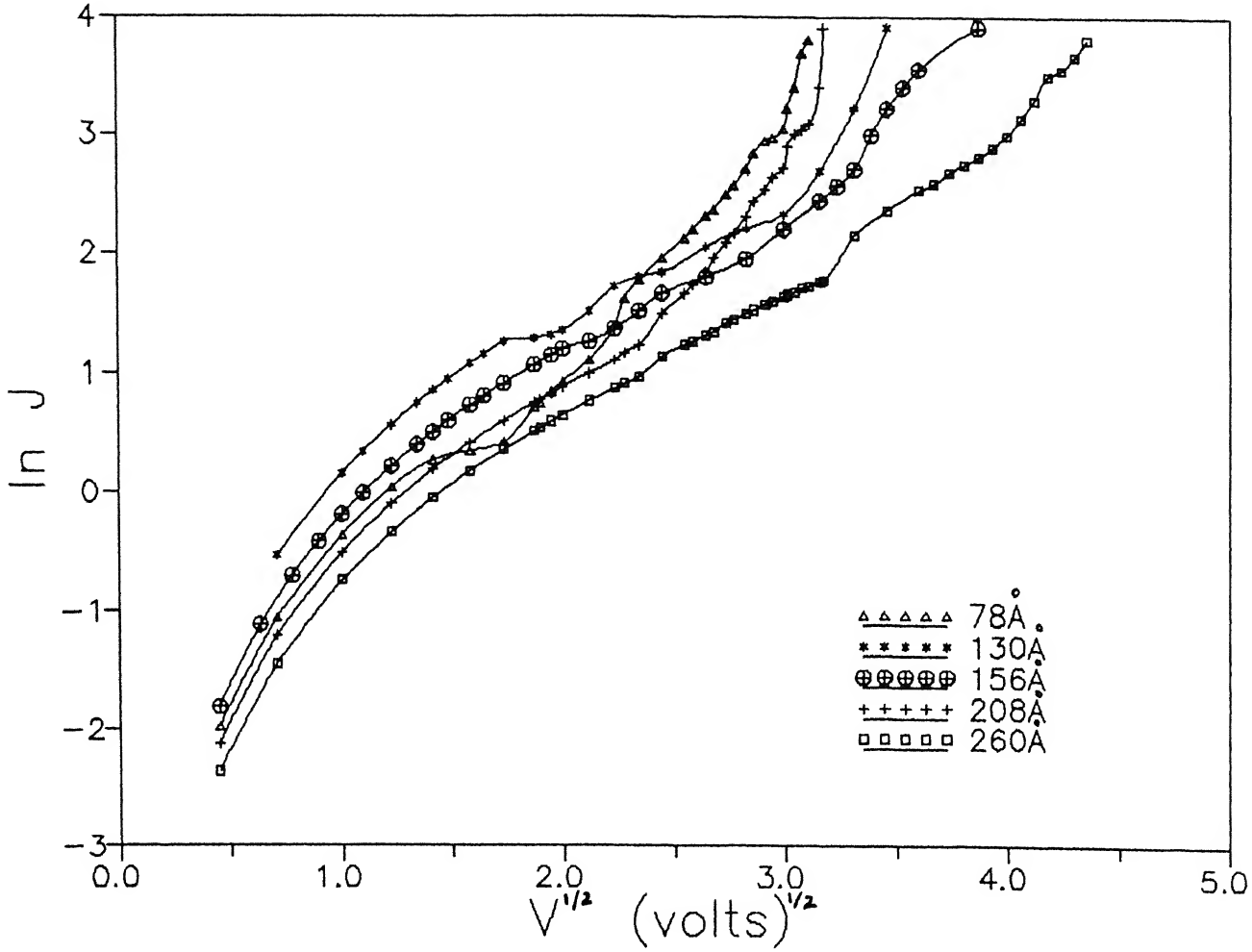

Fig.3.15 The ln J versus $V^{1/2}$ characteristics of Al-Al_2O_3-Al structures for various oxide thicknesses.

TABLE 3.4 VOLTAGE RANGES OF DIFFERENT CONDUCTION MECHANISMS

Oxide Thickness (A)	Ohmic (volts)	Schottky Emission (Volts)	Poole Frenkel Effect (Volts)	Field Emission (volts)
78	< 1.50	1.50-3.48	3.48-4.50	> 4.50
130	< 3.00	3.0-7.11	7.11-8.2	> 8.20
156	< 4.00	4.00-5.14	5.14-8.16	> 8.16
208	< 5.12	5.12-7.11	7.11-9.00	> 9.00
260	< 5.45	5.45-10.6	10.60	> 10.60

3.16).

With the help of intercepts at the ordinate of the extrapolated straight line fitted in the intermediate range of the voltage in ln J versus $V^{1/2}$ plots the barrier height (ϕ_o) can be evaluated [34]. Table 3.5 gives the value of ϕ_o obtained for the Al-Al_2O_3-Al samples of various oxide thicknesses which are in good agreement with those determined by Emptage & Tantrapon [33] and Antula [46]. Their values being Ø.7 eV and Ø.74 eV, respectively. Also the barrier height (ϕ_o) increases with the oxide thickness. The term ($\beta_{pf}/d^{1/2}$) for the Poole-Frenkel effect is evaluated from the slope of the straight line portion of the ln J/V versus $V^{1/2}$ plot. This is shown in fig 3.17 as a function of $d^{-1/2}$ The straight line representing the best fit and passing through the origin gives β_{pf} (field lowering coefficient) from its slope The value of β_{pf} comes out to be 1.Ø5 X $1Ø^{-5}$ $V^{1/2}m^{-1/2}$ and 2.1Ø X $1Ø^{-5}$ $V^{1/2}m^{-1/2}$ depending on taking eq.1.15 and 1.16, respectively. The theoretical value of β_{pf} as estimated from $\beta_{pf} = \{e^3/(\pi\varepsilon_o K^*)\}^{1/2}$ for K^* =9.Ø is 2.52 X $1Ø^{-5}$ $V^{1/2}m^{-1/2}$. This suggests that eq.1.16, which requires the presence of traps and donors in the insulator, gives the correct value of the current arising due to the Poole-Frenkel effect.

At high electric fields, the current density exhibits the following relationship with the voltage :.

$$\ln [J/v^2] = A - (B/V) \qquad \ldots.(3.4)$$

TABLE 3.5 DIFFERENT PARAMETERS OBTAINED FOR SCHOTTKY EMISSION

Anodisation Voltages (volts)	Oxide Thickness (A)	Barrier Height ϕ_o (eV)
6	78	Ø.652
1Ø	13Ø	Ø.676
12	156	Ø.683
16	2Ø8	Ø.69Ø
2Ø	26Ø	Ø.692

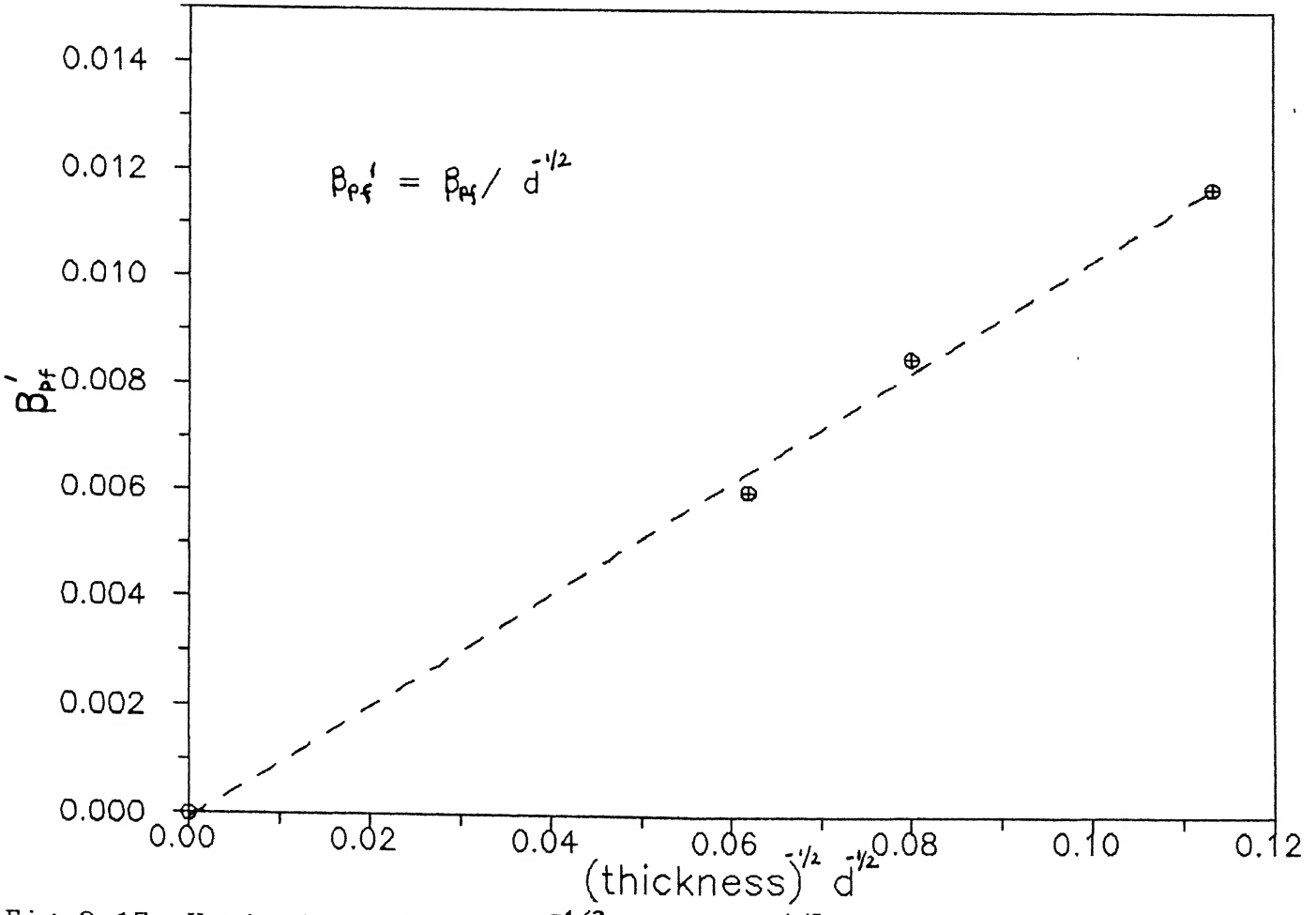

Fig.3.17 Variation of $\beta_{pf}/d^{-1/2}$ with $d^{-1/2}$; β_{pf} is the field lowering coefficient and d is the oxide thickness.

where A and B are constants. Hence the plot of ln $[J/V^2]$ as a function of 1/V should yield a straight line with a negative slope for the voltage range. This corresponds to the electron tunneling directly from one electrode to another through the oxide. The situation is analogous to that of field emission from a metal electrode. This conduction mechanism which is assisted by the field is called Fowler-Nordheim tunneling [47]. The ln $[J/V^2]$ versus 1/V plots derived from the measured data of all the samples under investigation, invariably show straight line with negative slope in the high field regime (Fig 3.18). Also, after a definite minimum they exhibit a positive slope. This minimum corresponds to the voltage at which the tunneling process involving field emission gets initiated. The electric field responsible in any case is very high. So, tunneling occurs, in which electrons from the top electrode pass directly to the bottom electrode (being positively biased). The presence of a definite minimum in the ln (J/V^2) versus 1/V plot is also taken as the criterion for the existence of Schottky emission (see, Table 3.4). However, the results given above favour the minimum just to represent the taking over point of the conduction by the tunneling process assisted by the strong electric field. Fig 3.19 summarizes schematically the various current processes found in the present investigation with their range of operation.

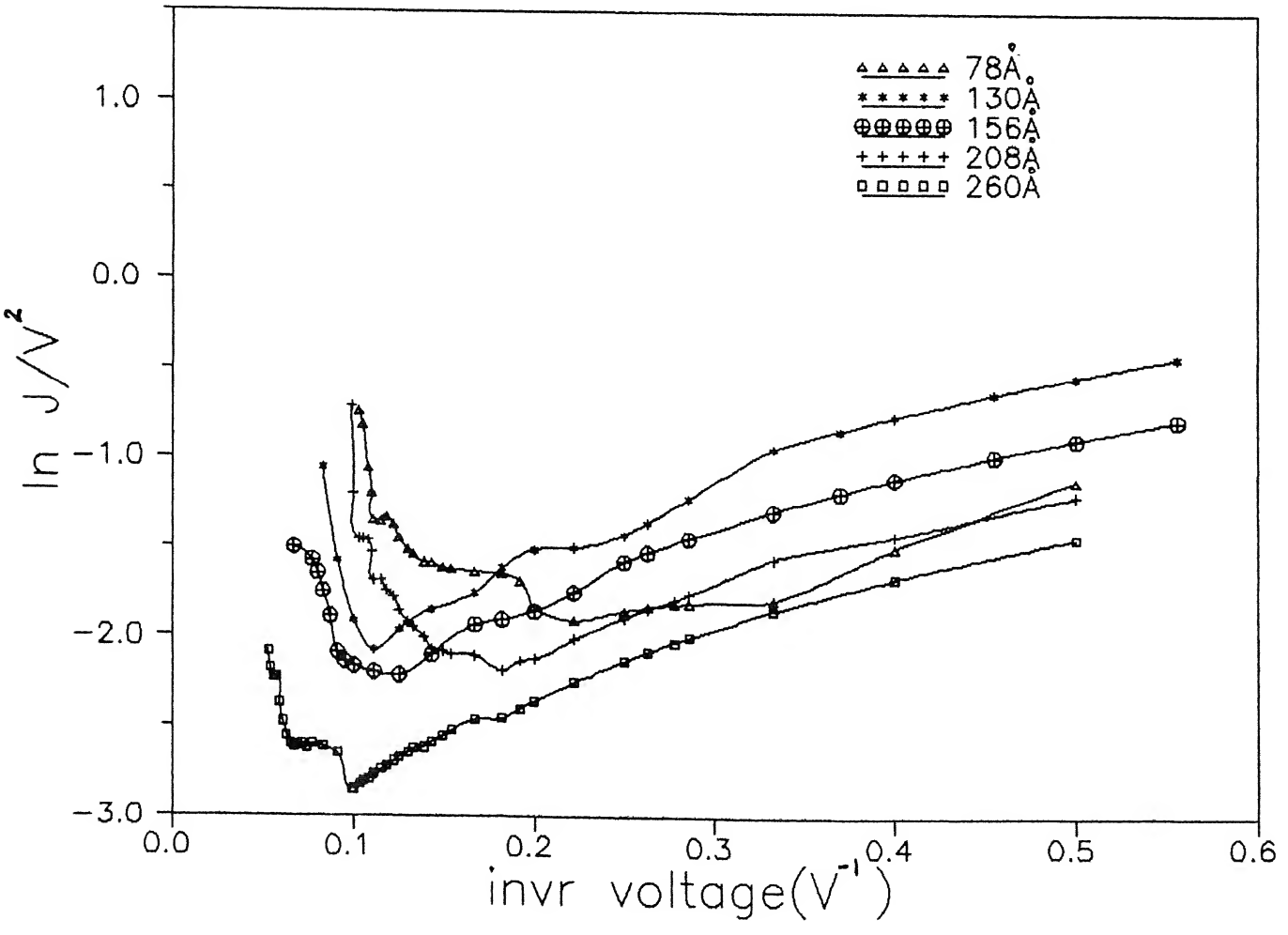

Fig.3.18 The ln J/V^2 versus 1/V characteristics of Al-Al_2O_3-Al structures for various oxide thicknesses.

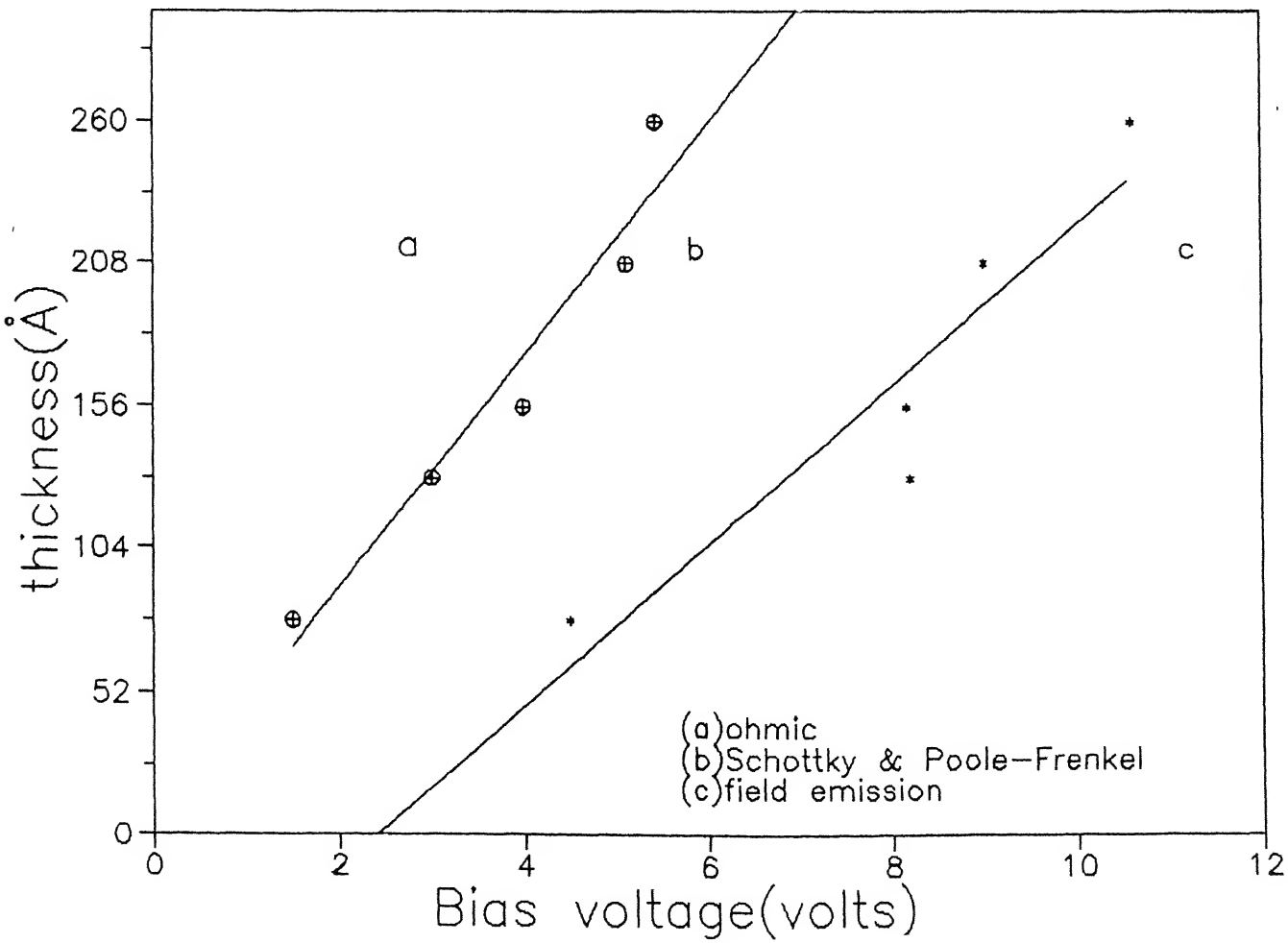

Fig.3.19 Various current processes found in Al-Al_2O_3-Al structures with their range of operation.

3.3.2 *Effect of polarity change*

The Al-Al_2O_3-Al samples have the same electrode metal (i.e., Al) on both sides of the dielectric. Yet, the J-V characteristics observed are found to be different on reversing the polarity of the electrodes. This behaviour was prevailing in all the Al-Al_2O_3-Al structures studied. A typical example is presented in fig (3.2Ø). As can be seen, that the threshold voltage (i.e., corresponding to initiation of non-linearity in J-V plots) becomes more pronounced when bottom electrode is positively biased.

Such a behaviour is expected because of the different interface nature on both sides of the oxide. The bottom metal which is anodized is in intimate contact with the oxide, whereas, the top electrode has an abrupt interface. The bottom electrode-oxide interface is assumed to have a transition region which may also behave like a semiconducting material. When the bottom electrode is negatively biased, because of the transition region, the barrier height decreases and the flow of electrons becomes easier. In this case electrons travel from the bottom electrode to the top one. But, when the top electrode is made negative, the electrons need to climb up the abrupt barrier of almost the same height and so constitute a small current towards the bottom electrode.

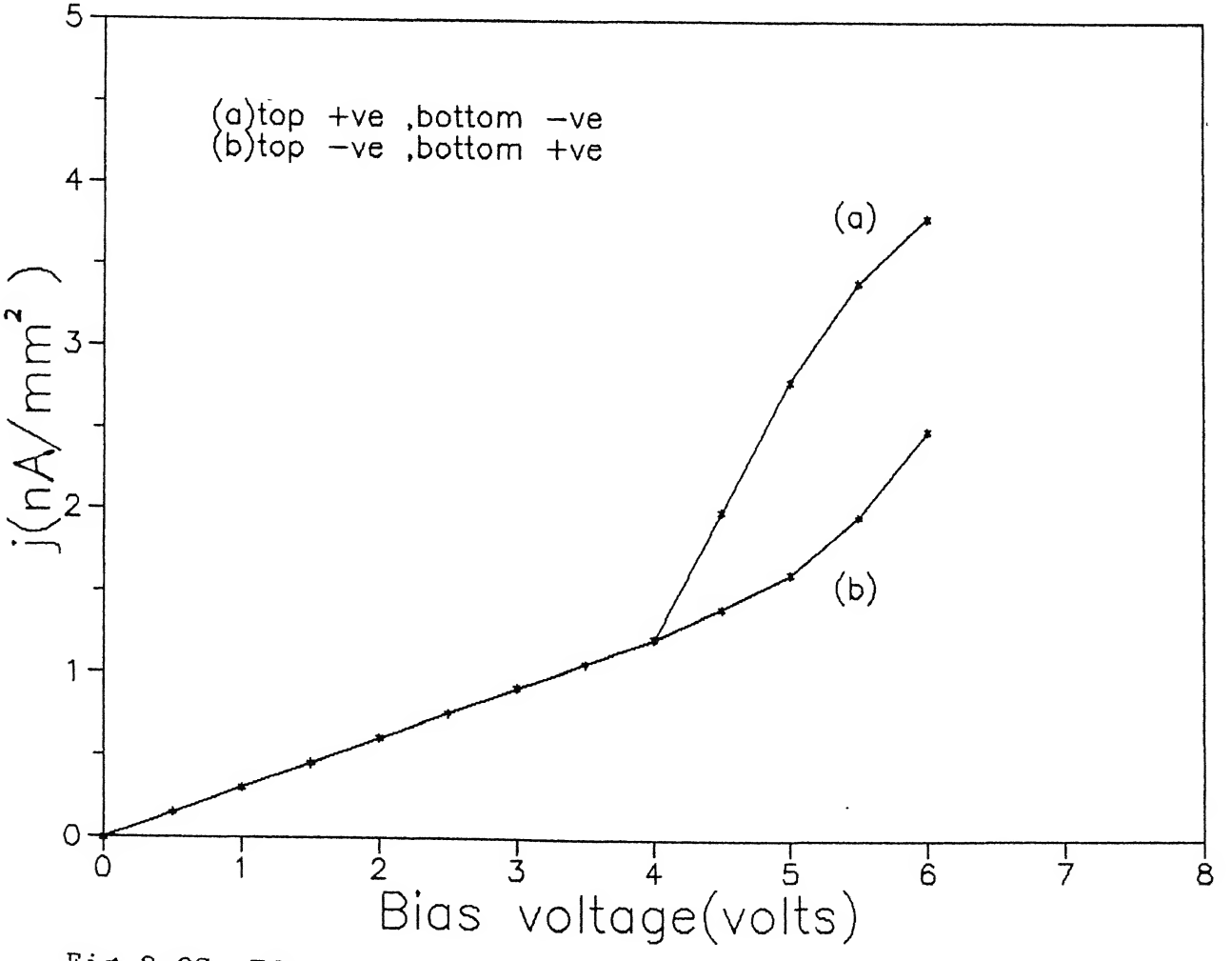

Fig.3.2Ø Effect of polarity change on J-V characteristics of $Al-Al_2O_3-Al$ structures.

3.3.3 *Hysteresis effects*

The current in $Al-Al_2O_3-Al$ structure varies non-linearly beyond the threshold voltage. After reaching some particular voltage higher than the threshold, the current has been measured by decreasing the bias. The current level now remains high and the original path cannot be retraced. This means that the hysteresis occurs. Such a behaviour was noticed in all the $Al-Al_2O_3-Al$ structures. Fig (3.21) shows a typical result of a sample of oxide thickness 156A. This result is quite similar to the observations reported in literature [47]. The presence of hysteresis suggests that some permanent change occurs in the bulk and/or interface when the electric field exceeds a particular value (corresponding to the initiation of the non-linearity in the J-V plot). Since, the current increases progressively and sharply, reasonable heating of oxide could also take place resulting in further changes. Evidence for such a conjecture is found from measurement again by increasing the bias. While the ohmic region is retraceable, the current in the non-linearity region lies in between the two situations dealt above.

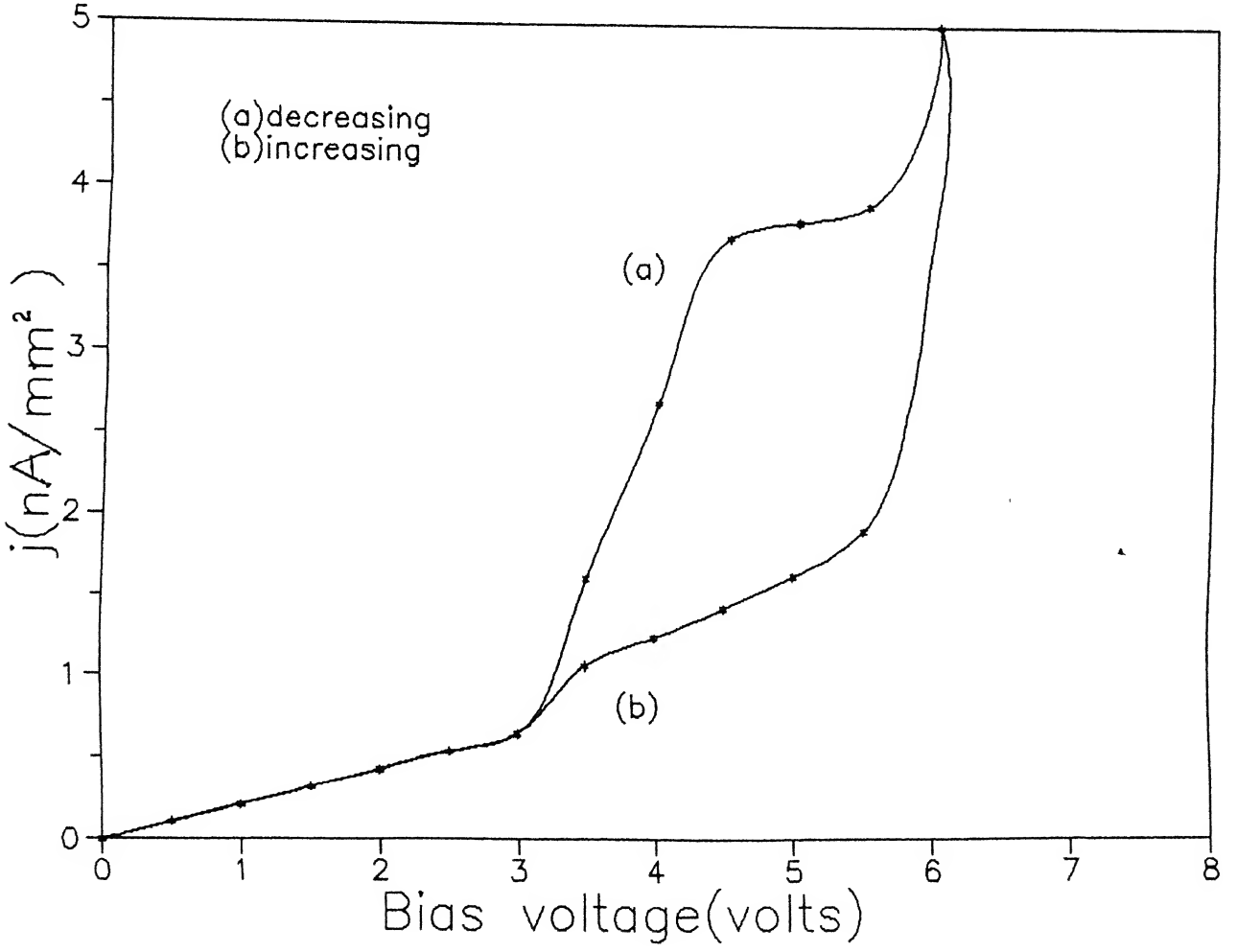

Fig.3.21 Effect of hysteresis on J-V characteristics of Al-Al_2O_3-Al structures.

4. CONCLUSIONS

1. Uniform, amorphous and non-porous Al_2O_3 films of controllable thickness in the range of 26-260 A can be prepared by anodization of the aluminium in 3 wt% tartaric acid solution of pH 5.5.

2. The inverse areal capacitance of $Al-Al_2O_3-Al$ trilayer structures varies linearly with oxide thickness (d) and gives a non-zero intercept at d = Ø. The capacitance corresponding to this intercept results due to interfacial effects and has a significant value (1.22 $\mu F/cm^2$), being equivalent to a bulk dielectric of size 1mm X 1mm X 62A.

3. Annealing of oxide films causes stress as well as the moisture removal and leads to stabilization of the dielectric capacitance.

4. Both the interfacial and total capacitance of $Al-Al_2O_3-Al$ trilayer structures increase directly with the junction area.

5. The slopes of the A/C_m versus `d' plots could be used to calculate the dielectric constant of the insulator. The dielectric constant (K) of anodized $Al_2O_3$ films increases with the heat treatment. For example, while the value of `K' of just anodized Al_2O_3 films is 8.5, it increases to 9.Ø and 1Ø.9 after heating in air for four hours at 16Ø°C and 2ØØ°C, respectively.

6. The J-V characteristics of Al-Al_2O_3-Al structures have two regimes. In the first, the current is very low ($\sim 10^{-9}$A) and samples show ohmic behaviour. This regime extends upto a threshold voltage such that a limiting electric field of $\sim 2.3 \times 10^{6}$ V/cm for all the samples regardless of the oxide thickness is established. The second regime involves a rapid increase in current for marginal increase in the applied voltage beyond the threshold value.

7. The possible conduction mechanisms operative in Al-Al_2O_3-Al structures are ohmic, Schottky-emission, Poole-Frenkel effect and field assisted tunneling, depending upon the bias.

8. The effect of polarity change on the Al-Al_2O_3-Al samples reveal that the barrier (at bottom interface) between the bottom electrode and the oxide is a graded type, while that between the top and the oxide is abrupt in nature.

9. The barrier height (ϕ_0) of Al-Al_2O_3-Al structures increases with oxide thickness and correspond to 0.65 and 0.69 eV for Al_2O_3 thickness of 78A and 260A, respectively. Also, the field lowering coefficient (β_{pf}) for the Poole-Frenkel effect is found to be 2.1×10^{-5} $V^{1/2}m^{-1/2}$.

REFERENCES

1. H.Biederman , *Vacuum*, 26, 513, (1976) .
2. C.A.Mead , *J.Appl.Phys.*, 32, 646, (1961) .
3. J.C.Fisher and I.J Giaver , *J. Appl. Phys.*, 32, 172, (1961) .
4. T.W.Hickmott , *J. Appl. Phys.*, 32, 2669, (1962) .
5. H.Birey , *J Appl. Phys.*, 48, 5209, (1977) .
6. A.K.Ray and C.A.Hogarth , *Int. J. Elec.*, 57, 1, (1984) .
7. R.R.Verderber , *Phil. Mag.*, 1, 1049, (1967) .
8. G.Dearnley , *J. Non-Cryst. Solids*, 4, 593, (1970) .
9. C.Barriac , *Phys. Stat. Solidi*, 34, 621, (1969) .
10. A.F.Hebard , *Appl. Phys.Lett.*, 51, 1349, (1987) .
11. S.R.Pollack and C.E.Morris , *J.Appl. Phys.*,35, 1503, (1964) .
12. C.A.Mead , *Phys. Rev. Lett.*, 6,545, (1961) .
13. H.Y.Ku and F.G.Ullman , *J. Appl. Phys.*, 35, 265,(1965) .
14. J.G.Simmons , *Appl. Phys. Lett.*, 6, 54, (1965) .
15. A.K.Theophilov and A.Modinos , *Phys.Rev.*, B6, 801, (1972) .
16. C.K.Chow , *J. Appl. Phys.*, 34, 25998, (1963) .
17. Z.Hurych , *Solid State Electronics*, 9, 967, (1966) .
18. J.Krupski , *Phys. Stat. Sol.(b)*, 157, 199, (1990) .
19. H.M.Gupta and M.B.Morris , *J. Appl.Phys.*,68, 176, (1990) .
20. J.G.Simmons , *J. Appl. Phys.*, 41, 538, (1970) .
21. J.G.Simmons , *J. Appl. Phys.*, D4, 613, (1971) .
22. H.Sambe and D.E.Ramekar , *J. Vac. Sc. Tech.*, A10, 2991, (1992) .
23. N.Schwartz and R.W.Berry ,*Physics of Thin Films*, G.Hass and R.E.Thun(Editors) , Academic Press, New York , (1980) .

24. G.Dearnley, *Rep. Prog. Prog. Phys.*, 33, 1129 (197Ø)

25. D.R.Lamb, *Electrical Conduction Mechanism in Thin Insulating Films*, Metheun and Co. Ltd., London,(1967) .

26. L.I.Maissal and R.Glang, *Handbook of Thin Film Technology* , McGraw - Hill Book Co., (197Ø) .

27. S.R.Pollack and J.A.Seitchik, *Applied Solid State Science Vol-1*, R.Wolfe and C.J.Kriessman (Editors), Academic Press, New York, (1969) .

28. J.G.Simmons, *J. Appl. Phys.*, 34, 1793, (1963) .

29. J.G.Simmons, *J. Appl. Phys.*, 34, 2581, (1963) .

3Ø. J.G.Simmons, *Tunneling Phenomenon in Solids* , E.Burstein and S.Lundquist(Editors), Plenum Press, New, (1969) .

31. D.V.Geppert, *J. Appl. Phys.* 34, 49Ø, (1963) .

32. R.Holm, *J. Appl. Phys.*, 22 ,569, (1965) .

33. P.R.Emptage and W.Tantraporn, *Phys. Rev. Lett.*, 8, 267, (1962) .

34. S.R.Pollack, *J. Appl. Phys.*, 34, 877, (1963) .

35. D.A.Vermilyea, *Acta Metallurgica.*, 2, 346, (1954) .

36. J.G.Simmons, *Phys. Rev.*, 155, 657, (1967) .

37. C.A.Mead, *Phys. Rev.*, 128, 2Ø88, (1962) .

38. N.F.Mott and R.W.Gurney, *Electronic Processes In Ionic Solids*, O.U.P., New York, (194Ø) .

39. A.Rose, *Phys. Rev.*, 97, 1538, (1955) .

4Ø. L.Young, *Anodic Oxide Films*, Academic Press, New York, (1961)

41. G.J.Hass, *J. Opt. Soc. Amer.*, 39, 532, (1949) .

42. J.Bernard, *Phys. Stat. Sol.*, 31, 315, (1969) .

43. K.R.Lawless, *Rept. Prog. Phys.*, 37, 231, (1974) .

44. H.S.Hunter and P.J.Fowle, *J. Electrochem. Soc.*, 1Ø1, 514,

(1954) .

45. S.M.Vaezi-Nijad, *Int. J.* Int. *Electronics*, 68, 59, (1990).

46. J.Antula, *Phys. Lett. A.*, 25A, 309, (1967) .

47. A.Roy Bardhan, *Int. J. Electronics*, 40,313. (1976) .

48. F.M.Nazar and N.Ahmed, *Thin Solid Films.*, 81,(1979) .

49. L.Vijayraghavan, *Electrical Characteristics of Thermally Grown* Al_2O_3 *Films*, M.Tech. Thesis , I.I.T.Kanpur ,(1990)

50. G.Swaminathan, *Studies of Electrical and Dielectric Properties of* Al-Al_2O_3-Al *Trilayer Structures*, M.Tech.Thesis, I.I.T.Kanpur ,(1993)

MSP-1994-M-SIN-ELE